Postprint of: Dziedzic J., Bhandari A., Anton L., Peng C., Womack J., Famili M., Kramer D., Skylaris C., Practical Approach to Large-Scale Electronic Structure Calculations in Electrolyte Solutions via Continuum-Embedded Linear-Scaling Density Functional Theory, Journal of Physical Chemistry C, Vol. 124, iss. 14 (2020), pp. 7860-7872.

A Practical Approach to Large Scale Electronic Structure Calculations in Electrolyte Solutions via Continuum-Embedded Linear-Scaling DFT

Jacek Dziedzic,[†,‡,¶] Arihant Bhandari,[†,¶] Lucian Anton,[§] Chao Peng,[‖,¶] James Womack,[†,¶] Marjan Famili,[†,¶] Denis Kramer,[‖,¶,⊥] and Chris-Kriton Skylaris*[,†,¶]

†*School of Chemistry, University of Southampton, Highfield, Southampton SO17 1BJ, United Kingdom*

‡*Faculty of Applied Physics and Mathematics, Gdansk University of Technology, Gdansk 80-233, Poland*

¶*The Faraday Institution, Quad One, Becquerel Avenue, Harwell Campus, Didcot, OX11 0RA, UK*

§*CCFE, Culham Science Centre, Abingdon, UK*

‖*Engineering Sciences, University of Southampton, Southampton SO17 1BJ, United Kingdom*

⊥ *Helmut-Schmidt-University, University of the Armed Forces, 22043 Hamburg, Germany*

E-mail: C.Skylaris@soton.ac.uk

Abstract

We present the implementation of a hybrid continuum-atomistic model for including the effects of surrounding electrolyte in large-scale density functional theory (DFT) calculations within the ONETEP linear-scaling DFT code, which allows the simulation of large complex systems such as electrochemical interfaces. The model represents the

electrolyte ions as a scalar field and the solvent as a polarisable dielectric continuum, both surrounding the quantum solute. The overall energy expression is a grand canonical functional incorporating the electron kinetic and exchange correlation energies, the total electrostatic energy, entropy and chemical potentials of surrounding electrolyte, osmotic pressure, and the effects of cavitation, dispersion and repulsion. The DFT calculation is performed fully self-consistently in the electrolyte model, allowing the quantum mechanical system and the surrounding continuum environment to interact and mutually polarize. A bespoke parallel Poisson-Boltzmann solver library, DL_MG, deals with the electrostatic problem, solving a generalized Poisson-Boltzmann equation. Our model supports open boundary conditions, which allows the treatment of molecules, entire biomolecules or larger nanoparticle assemblies in electrolyte. We have also implemented the model for periodic boundary conditions, allowing the treatment of extended systems such as electrode surfaces in contact with electrolyte. A key feature of the model is the use of solute-size and solvation-shell-aware accessibility functions that prevent the unphysical accumulation of electrolyte charge near the quantum solute boundary. The model has a small number of parameters—here we demonstrate their calibration against experimental mean activity coefficients. We also present an exemplar simulation of a 1634-atom model of the interface between a graphite anode and $LiPF_6$ electrolyte in ethylene carbonate solvent. We compare the cases where Li atoms are intercalated at opposite edges of the graphite slab and in solution, demonstrating a potential application of the model in simulations of fundamental processes in Li-ion batteries.

Introduction

Solid-liquid interfaces are frequently encountered in biology, chemistry, physics, materials science and engineering. The effect of solvent on the surface-energetics is quite important to the extent that it can yield negative surface energies for alumina in water resulting in a highly porous structure.[1] Moreover, many practical reactions occur in electrolytic solutions, which

contain finite concentration of ionic charges in the solvent, where the effect of electrolyte concentrations affects the energetics at the interface. Therefore, in order to model the energetics at the interface correctly, one needs to carefully consider the effect of environment (the electrolyte solution) around the system (solute), which can be, for example, a metal surface in catalytic applications, a protein in case of biological systems, or an electrode in a battery in contact with the electrolyte solution.

Quantum-mechanical methods such as density functional theory (DFT) have been successful in describing the electronic properties of molecules and materials.[2,3] The associated computational cost grows as order $O(N^3)$ in conventional DFT (where N is the number of atoms in the system). More recent reformulations of DFT allow reduced or linear-scaling computational cost as is the case in the Order-N Electronic Total Energy Package (ONETEP)[4] program.

In the case where the material studied with DFT is in contact with a solvent, which might also contain electrolyte, the explicit description of the electrolyte solution can be computationally prohibitive due to the large number of solvent and electrolyte molecules and the need to average over all possible degrees of freedom. Often, the focus area or the region of interest is the solute, or solid side of the interface, and one only wants to estimate the mean field effect of the electrolytic solution. Hence, an explicit or discrete representation of the electrolyte solution can be replaced by a dielectric continuum with a continuously varying charge density of the mobile electrolyte ions. Hybrid quantum-mechanical/continuum solvation models treat the solute quantum mechanically and the surrounding solution at a classical continuum level.[5] The quantum problem deals with the determination of the electronic density (ρ_e) of a given arrangement of nuclei in the presence of an external potential (ν) by solving the Kohn-Sham equations. The classical problem deals with finding the electrostatic potential (ν) given the total charge density by solving a Poisson-Boltzmann equation (P-BE) (which includes the charge density due to mobile electrolyte ions). This is a non-linear coupled formalism which requires the simultaneous solutions of both equations.

Different approaches have been reported to address the electrostatic problem in pure solvent, which include the polarizable continuum model (PCM) pioneered by Tomasi,[6,7] conductor-like screening model (COSMO) devised by Klamt and Schüürmann,[8] integral equation formalism (IEF) originally developed by Cances and Mennucci,[9] surface and volume polarization for electrostatics (SVPE) by Chipman and coworkers,[10] multipole expansion methods (MPE) by Kirkwood[11] and Onsager,[12] generalized Born methods,[13,14] finite element methods,[15] finite difference methods,[16] multigrid methods,[17] etc. A major theoretical advancement in the field came through the isodensity polarizable continuum model (IPCM) proposed by Foresman,[18] and the model for a smooth dielectric function proposed by Fattebert and Gygi,[19] which replaced the rigid dielectric cavity by a smoothly varying dielectric function described in terms of the electronic density of the quantum solute. This was further extended by Scherlis *et al.* (FGS model) to include the cavitation energy.[20] A variant of the FGS model was implemented by Dziedzic *et al.* in ONETEP[21,22] ("minimal-parameter solvent model" or MPSM) which included dispersion-repulsion contributions, and a parametrization that produced accurate solvation energies for neutral molecules as well as cations and anions while overcoming the issue of numerical convergence of the FGS model. The dielectric function proposed in the FGS model was further revised in the self consistent continuum solvation (SCCS) model by Andreussi,[23] where a different parametric form for the dielectric function was chosen to improve numerical convergence via a self consistent iterative procedure.

In the presence of electrolyte, the solutions to the P-BE lead to unphysical electrolyte charge accumulation near the solute.[24,25] Several approaches for addressing this problem have been proposed – e.g. adjusting the entropy density expression to account for the finite size of the mobile ions,[26,27] additionally introducing a repulsive potential between the solute and the electrolyte,[28] or (equivalently) employing exclusion functions,[29,30] or making the maximum ionic concentration space-dependent.[31]

Here, we present an implementation of an electrolyte implicit solvent model which is

based on the solvent model of the ONETEP code (MPSM). We describe the underlying theory, including how we prevent the problem of excessive electrolyte charge accumulation near the boundary of the quantum solute by including regions inaccessible to the electrolyte ions. We develop the model for open boundary conditions but also for fully periodic boundary conditions, which, to our knowledge, is the first time that an electrolyte implicit solvent model in DFT has been developed to be able to work with these boundary conditions. We also develop linearized approximations of the model for both of these boundary conditions. Then we develop formulas for the free energy of solvation of a substance in electrolyte. We describe the details of the implementation of our model within the ONETEP code and the DL_MG bespoke parallel Poisson-Boltzmann solver library, which allow DFT calculations with thousands of atoms. We also give examples of the parametrisation of the model using experimental mean activity coefficients. Finally, we present an example calculation on a graphite-Li system to demonstrate one potential use of our model which could involve the simulation of solid-electrolyte interfaces as is the case with electrochemical systems such as battery electrodes. We conclude with some suggestions for applications and future developments.

Theory

System

Our model belongs to the class of quantum-continuum solvation models that split the system into two subsystems – the quantum system and the continuum system:

$$\rho_{\mathrm{tot}}(\mathbf{r}) = \underbrace{\rho(\mathbf{r})}_{\text{quantum}} + \underbrace{\rho_{\mathrm{mob}}(\mathbf{r})}_{\text{continuum}}, \tag{1}$$

where ρ is the charge density of the quantum system, ρ_{mob} is the charge density of the mobile electrolyte ions and ρ_{tot} is the total charge density. The quantum system includes pseudopo-

tential cores and valence electrons. Further, under the Born-Oppenheimer approximation,[32] we assume the ionic cores are fixed.

$$\rho(\mathbf{r}) = \rho_{\mathrm{e}}(\mathbf{r}) + \rho_{\mathrm{nuc}}(\mathbf{r})\,, \tag{2}$$

where, ρ_{e} is the charge density due to electrons and ρ_{nuc} is the charge density due to ionic cores. The continuum system includes the representation of the solvent as a dielectric medium and of the (mobile) electrolyte ions as an ideal solution. We assume the electrolyte comprises p mobile ion species, with charges $\{z_i\}$, and local (position-dependent) concentrations $\{c_i(\mathbf{r})\}$, $i = 1 \ldots p$. The charge density of mobile ions is thus given by:

$$\rho_{\mathrm{mob}}(\mathbf{r}) = \sum_{i=1}^{p} z_i c_i(\mathbf{r})\,. \tag{3}$$

Free Energy Functional

Expressions for free energy, with a number of ways to group the terms, have been given by, *inter alia*, Sharp and Honig,[33] Fogolari *et al.*,[34] Grochowski and Trylska,[24] Jinnouchi and Anderson,[28] Mathew and Hennig,[35] Ringe *et al.*,[29] Gray and Stiles,[36] and Nattino *et al.*[31] We feel obliged to point out that subtle differences in the assumptions made by different authors (differing boundary conditions; whether accessibility is taken into account, and if so, if it is limited to discrete values of 0 and 1, or if it is a continuous function; whether the argument in the exponentials are "capped" during the numerical solution procedure to avoid floating-point overflows, etc.) mean utmost care should be taken when implementing or comparing different derivations, particularly when they rely on some of the terms canceling out. Following Jinnouchi,[28] Ringe[29] and Gray,[36] we construct a grand potential which is a functional of the electronic density (ρ_{e}), electrolyte concentrations $\{c_i\}$ and the electrostatic

potential (ν) as:

$$\Omega\left[\rho_{\mathrm{e}},\{c_i\},\nu\right]=T_{\mathrm{s}}\left[\rho_{\mathrm{e}}\right]+E_{\mathrm{xc}}\left[\rho_{\mathrm{e}}\right]-TS_{\mathrm{e}}+V_{\mathrm{ps}}\left[\rho_{\mathrm{e}}\right]+\Omega_{\mathrm{mf}}\left[\rho_{\mathrm{e}},\{c_i\},\nu\right]+\Omega_{\mathrm{nmf}}\left[\rho_{\mathrm{e}}\right], \tag{4}$$

where the terms on the right hand side (RHS) are the kinetic energy of electrons (T_{s}), the exchange-correlation energy (E_{xc}), contribution from electronic entropy ($-TS_{\mathrm{e}}$),[37] the contribution due to the pseudopotentials (V_{ps}), the mean-field contributions (Ω_{mf}), and the non-mean-field contribution due to cavitation, solute-solvent dispersion and repulsion (Ω_{nmf}). The mean field contributions include:

$$\Omega_{\mathrm{mf}}\left[\rho_{\mathrm{e}}(\mathbf{r}),\{c_i(\mathbf{r})\},\nu(\mathbf{r})\right]=U^{\mathrm{elec}}+U^{\mathrm{osmo}}+U^{\mathrm{acc}}-T\sum_{i=1}^{p}\int_V s\left[c_i(\mathbf{r})\right]\mathrm{d}\mathbf{r}-\sum_{i=1}^{p}\mu_i N_i, \tag{5}$$

where all the integrals are over the volume of the simulation cell. We will now elaborate each of the terms on the RHS. Atomic units are used everywhere. The electrostatic energy (U^{elec}) can be written as:[33]

$$U^{\mathrm{elec}}\left[\rho_{\mathrm{e}}(\mathbf{r}),\nu(\mathbf{r})\right]=\int_V\left[-\frac{\mathbf{E}(\mathbf{r})\cdot\mathbf{D}(\mathbf{r})}{2}+\rho(\mathbf{r})\,\nu(\mathbf{r})+\sum_{i=1}^{p}z_i c_i(\mathbf{r})\,\nu(\mathbf{r})\right]\mathrm{d}\mathbf{r} \tag{6}$$

The first term under the integral on the RHS is the electrostatic stress, which, given that $\mathbf{E}=-\nabla\nu$ and that the electric displacement $\mathbf{D}=\varepsilon\dfrac{\mathbf{E}}{4\pi}$, can be written as:

$$\frac{\mathbf{E}(\mathbf{r})\cdot\mathbf{D}(\mathbf{r})}{2}=\frac{\varepsilon(\mathbf{r})}{8\pi}|\nabla\nu(\mathbf{r})|^2. \tag{7}$$

Hence, the electrostatic energy can be written as:

$$U^{\mathrm{elec}}\left[\rho_{\mathrm{e}}(\mathbf{r}),\nu(\mathbf{r})\right]=\int_V\left[-\frac{\varepsilon(\mathbf{r})}{8\pi}|\nabla\nu(\mathbf{r})|^2+\rho(\mathbf{r})\,\nu(\mathbf{r})+\sum_{i=1}^{p}z_i c_i(\mathbf{r})\,\nu(\mathbf{r})\right]\mathrm{d}\mathbf{r} \tag{8}$$

Further, the last two terms in Eq. (6) are related to the electrostatic stress by a restatement of Gauss's law,[33] namely:

$$\int_V \frac{\mathbf{E}(\mathbf{r}) \cdot \mathbf{D}(\mathbf{r})}{2} \mathrm{d}\mathbf{r} = \frac{1}{2} \int_V \left[\rho(\mathbf{r})\, \nu(\mathbf{r}) + \sum_{i=1}^{p} z_i c_i(\mathbf{r})\, \nu(\mathbf{r}) \right] \mathrm{d}\mathbf{r}. \tag{9}$$

Hence, the electrostatic energy can be rewritten as:

$$U^{\mathrm{elec}} \left[\rho_{\mathrm{e}}(\mathbf{r}) \,, \nu(\mathbf{r}) \right] = \int_V \frac{1}{2} \left[\rho(\mathbf{r})\, \nu(\mathbf{r}) + \sum_{i=1}^{p} z_i c_i(\mathbf{r})\, \nu(\mathbf{r}) \right] \mathrm{d}\mathbf{r} \tag{10}$$

The dielectric permittivity ($\varepsilon(\mathbf{r})$) that appears in Eq. (8), is defined in terms of the vacuum electronic density ($\rho_{\mathrm{e}}^{\mathrm{vac}}$) as:[21]

$$\varepsilon(\mathbf{r}) = 1 + \frac{\varepsilon_{\mathrm{bulk}} - 1}{1 + \left(\rho_{\mathrm{e}}^{\mathrm{vac}}(\mathbf{r}) \,/ \rho_{\mathrm{e}}^{0} \right)^{2\beta}}, \tag{11}$$

where ρ_{e}^{0} and β are the parameters of the model (see Ref. 22 for the values used) and $\varepsilon_{\mathrm{bulk}}$ is the permittivity of the pure solvent. This is similar to the form proposed by Fattebert and Gygi,[19] except that it uses the vacuum electronic density ($\rho_{\mathrm{e}}^{\mathrm{vac}}$) rather than the self-consistent electronic density (ρ_{e}). While, in principle, it is possible to use a self-consistent dielectric function, we found in our earlier work (Ref. 21) that keeping the dielectric permittivity (solute cavity) fixed avoids the numerical stability issues of the form proposed by Fatterbert and Gygi.

The second term in Ω_{mf} (Eq. 5) is the osmotic pressure of the ideal solution of mobile electrolyte ions:

$$U^{\mathrm{osmo}} \left[\{ c_i(\mathbf{r}) \} \right] = -k_{\mathrm{B}} T \sum_{i=1}^{p} \int_V c_i(\mathbf{r})\, \mathrm{d}\mathbf{r}. \tag{12}$$

The ideal solution of mobile electrolyte ions suffers from a well-known deficiency (due to the lack of Pauli repulsion between the electrolyte ions and the solute)[24,25] whereby the electrolyte charge tends to accumulate near the solute, leading to unphysically large electrolyte concentrations. Our model circumvents this problem by defining an *accessibility function*,

$\lambda(\mathbf{r})$, $\lambda \in [0,1]$, which dictates which regions of space are fully accessible to mobile ions ($\lambda = 1$), partially accessible ($0 < \lambda < 1$), or entirely inaccessible ($\lambda = 0$). Accessibility can be thought of in terms of a repulsive *steric potential (energy)* $V^{\text{steric}}(\mathbf{r}) = -k_{\text{B}}T \ln \lambda(\mathbf{r})$ that mobile ions experience wherever $\lambda(\mathbf{r}) < 1$. Correspondingly, the third term in Ω_{mf} (Eq. 5) is the accessibility repulsion term, which is the same as Eq. 23 of Nattino *et al.*[31]

$$U^{\text{acc}}\left[\{c_i(\mathbf{r})\}\right] = \sum_{i=1}^{p} \int_V c_i(\mathbf{r})\, V^{\text{steric}}(\mathbf{r})\, \mathrm{d}\mathbf{r} = -k_{\text{B}}T \sum_{i=1}^{p} \int_V c_i(\mathbf{r}) \ln \lambda(\mathbf{r}) \mathrm{d}\mathbf{r}. \tag{13}$$

For the ionic accessibility $\lambda(\mathbf{r})$, we use the following model of interlocking spheres around each atom center ($\mathbf{R}_k$):[38–40]

$$\lambda(\mathbf{r}) = \prod_{k}^{n_{\text{atoms}}} \frac{1}{2} \left[1 + \text{erf}\left(\frac{|\mathbf{r} - \mathbf{R}_k| - R_k^{\text{solute}}(\rho_{\text{e}}^{\lambda}) - R_k^{\text{solvent}}}{\sigma} \right) \right], \tag{14}$$

where σ is a smearing width ($0 < \sigma < 0.5\ a_0$). Thus, the accessible region is defined by atom-centered interlocking spheres with smoothed boundaries. The product of the accessibility functions centered around each atom determines the overall accessibility function. Our description for the radius of interlocking spheres derives from a physical picture: the electrolyte ions are restricted from the quantum solute up to a distance that incorporates not only the solute size but also a solvent radius.

The solute radius around each atom is described in terms of an isovalue of vacuum electronic density ($\rho_{\text{e}}^{\lambda}$), which serves to free the model from a dependence on a large number of parameters (radii for every atomic species present). To do this, we use ONETEP's pseudoatomic solver functionality,[41] which determines the single-electron Kohn-Sham states for an isolated pseudoatom (of every species present). This method is used in ONETEP to generate robust initial guesses for the localised orbitals referred to as the Non-orthogonal Generalized Wannier Functions (NGWFs).[42] Here we use the fact that it produces radial density profiles for every species to determine the sphere radius that corresponds to a given electronic density isovalue. This density isovalue parameter (ρ_e^{λ}) is the only parameter of

this part of the model.

The solvent radius ($\{R_k^{\text{solvent}}\}$), which represents (an approximately rigid) first solvation shell for each electrolyte, is added to the solute radius to calculate the overall radius of interlocking spheres in our model for accessibility function. Both the parameters of our model: the isovalue of the vacuum electronic density ($\rho_{\text{e}}^{\lambda}$) and the solvation radius ($\{R_k^{\text{solvent}}\}$) are obtained by calibrating the computed mean activity coefficients of electrolytic solutions with experimental data. Aqueous solutions are expected to have a smaller solvation shell radius, due to the small size of water molecules, in contrast to organic solvents with larger steric sizes.

The fourth term in Ω_{mf} (Eq. 5) is the entropic contribution from the ideal non-uniform electrolyte solution:

$$-T\sum_{i=1}^{p}\int_{V} s\left[c_i(\mathbf{r})\right]\mathrm{d}\mathbf{r} = k_{\text{B}}T\sum_{i=1}^{p}\int_{V} c_i(\mathbf{r})\ln\left(\frac{c_i(\mathbf{r})}{c^{\circ}}\right)\mathrm{d}\mathbf{r}, \tag{15}$$

where c° is the standard thermodynamic reference of 1 mol/L or 1M.

The last term in Ω_{mf} (Eq. 5) is the chemical potential term that controls the number of particles (N_i) of the mobile electrolyte ions in the grand potential:

$$-\sum_{i=1}^{p}\mu_i N_i = -\sum_{i=1}^{p}\mu_i\int_{V} c_i(\mathbf{r})\,\mathrm{d}\mathbf{r}, \tag{16}$$

where μ_i is the chemical potential of species i, that is obtained from the boundary conditions (derived in the next subsection).

Our solvation model also includes the following non-mean-field contributions (Ω_{nmf}): cavitation, solute-solvent dispersion and repulsion. For the cavitation term we follow Scherlis *et al.*[20] and assume it is proportional to the surface area of the cavity. Solute-solvent dispersion and repulsion terms are included approximately, under the assumption that their combined value is also proportional to the surface area of the cavity, which leads to a simple

rescaling of the cavitation term:

$$\Omega_{\mathrm{nmf}} = kA, \tag{17}$$

where k is the rescaled surface tension and A is the solvent-accessible surface area.[21] The surface area is calculated from the isosurface of dielectric permittivity calculated at $\rho_{\mathrm{e}}^{\mathrm{vac}} = \rho_{\mathrm{e}}^{0}$.

Minimizing the grand potential functional with respect to the electronic density gives the Kohn-Sham equations:

$$\left[-\frac{1}{2}\nabla^2 + \nu_{\mathrm{ps}}(\mathbf{r}) + \nu(\mathbf{r}) + \frac{\delta E_{\mathrm{xc}}}{\delta \rho_{\mathrm{e}}}\right] \psi_i(\mathbf{r}) = \epsilon_i \psi_i(\mathbf{r})\,. \tag{18}$$

where ψ_i are the eigenfunctions (molecular orbitals or bands) with eigenvalues ϵ_i. Minimizing the grand potential functional with respect to the electrostatic potential $\nu(\mathbf{r})$ gives the generalized Poisson equation (GPE):

$$\nabla \cdot (\varepsilon(\mathbf{r})\, \nabla \nu(\mathbf{r})) = -4\pi \left[\rho(\mathbf{r}) + \sum_{i=1}^{p} z_i c_i(\mathbf{r})\right]. \tag{19}$$

Minimizing the grand potential functional with respect to ion concentrations $\{c_i(\mathbf{r})\}$ gives:

$$z_i \nu(\mathbf{r}) - k_{\mathrm{B}}T + V^{\mathrm{steric}}(\mathbf{r}) + k_{\mathrm{B}}T \ln\left(\frac{c_i(\mathbf{r})}{c^{\circ}}\right) + k_{\mathrm{B}}T - \mu_i = 0,\ i = 1 \ldots p. \tag{20}$$

On rearranging, the concentrations can be described in terms of chemical potentials as:

$$c_i(\mathbf{r}) = c^{\circ} \lambda(\mathbf{r}) \exp\left(-\frac{z_i \nu(\mathbf{r})}{k_{\mathrm{B}}T} + \frac{\mu_i}{k_{\mathrm{B}}T}\right),\ i = 1 \ldots p \tag{21}$$

The equations 18, 19 and 21 need to be solved self-consistently. The values of the chemical potentials are determined from the boundary conditions as described in the next section. We note here that substituting the expression for concentrations (Eq. 21) in the entropy expression (Eq. 15) simplifies the mean field free energy functional Ω_{mf} (Eq. 5) to:

$$\Omega_{\mathrm{mf}}\left[\rho(\mathbf{r})\,,\{c_i(\mathbf{r})\},\nu(\mathbf{r})\right] = \int_V \left[-\frac{\varepsilon(\mathbf{r})}{8\pi}|\nabla\nu(\mathbf{r})|^2 + \rho(\mathbf{r})\,\nu(\mathbf{r}) - k_{\mathrm{B}}T\sum_{i=1}^{p} c_i(\mathbf{r})\right]\mathrm{d}\mathbf{r}$$
$$= \int_V \left[\frac{1}{2}\rho(\mathbf{r})\,\nu(\mathbf{r}) - \frac{1}{2}\sum_{i=1}^{p} z_i c_i(\mathbf{r})\,\nu(\mathbf{r}) - k_{\mathrm{B}}T\sum_{i=1}^{p} c_i(\mathbf{r})\right]\mathrm{d}\mathbf{r}. \qquad (22)$$

A recent study by Stein *et al.* derives the same mean field free energy functional as in Eq. 22 by recasting the Poisson-Boltzmann Equation into a Euler-Lagrange equation.[40] Substituting the expression for concentrations (Eq. 21) in the GPE (Eq. 19) gives the general Poisson-Boltzmann Equation (P-BE):

$$\nabla\cdot\left(\varepsilon(\mathbf{r})\,\nabla\nu(\mathbf{r})\right) = -4\pi\left[\rho(\mathbf{r}) + \sum_{i=1}^{p} z_i c^{\circ}\lambda(\mathbf{r})\exp\left(-\frac{z_i\nu(\mathbf{r})}{k_{\mathrm{B}}T} + \frac{\mu_i}{k_{\mathrm{B}}T}\right)\right]. \qquad (23)$$

Boundary Conditions

A. Periodic Boundary Conditions (PBCs)

A schematic of a simulation cell which obeys periodic boundary conditions (PBCs) is shown in Figure 1, where the system $(\rho, \rho_{\mathrm{mob}})$ interacts with its periodic images $(\rho',\ \rho'_{\mathrm{mob}})$. The periodic boundaries are implemented in DL_MG via the minimum image convention (MIC).[43] MIC ensures that the electrostatic potential is due to the periodic system, rather than the isolated system. This approach also ensures continuity across the boundary and periodicity in $\nu(\mathbf{r})\,,\lambda(\mathbf{r})$ and therefore $c_i(\mathbf{r})$ and $\rho_{\mathrm{mob}}(\mathbf{r})$. The other consequence of the periodic boundary is on the total number of electrolyte ions.

In a periodically repeating cell, such as in Figure 1, the bulk concentration of electrolyte ions (c_i^{bulk}) is defined as the number of electrolyte ions N_i per the volume accessible to electrolyte ions $V_{\mathrm{acc}} = \int_V \lambda(\mathbf{r})\,\mathrm{d}\mathbf{r} = \Gamma V$ inside the cell:

$$c_i^{\mathrm{bulk}} = \frac{N_i}{V_{\mathrm{acc}}} = \frac{1}{V_{\mathrm{acc}}}\int_V c_i(\mathbf{r})\,\mathrm{d}\mathbf{r} = \frac{1}{\Gamma V}\int_V c^{\circ}\lambda(\mathbf{r})\exp\left(-\frac{z_i\nu(\mathbf{r})}{k_{\mathrm{B}}T} + \frac{\mu_i}{k_{\mathrm{B}}T}\right)\mathrm{d}\mathbf{r}. \qquad (24)$$

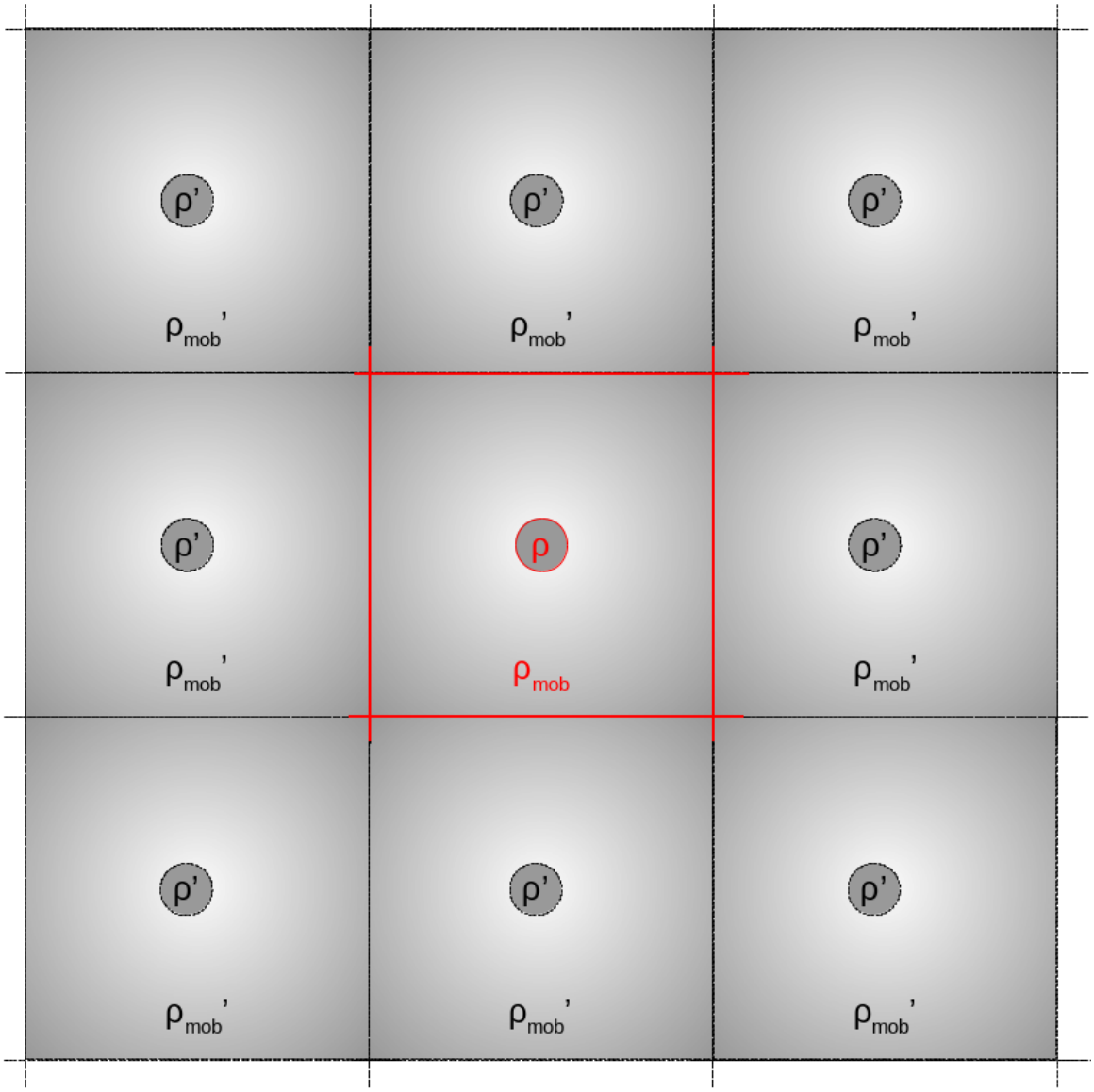

Figure 1: Schematic of a periodic cell (red) of quantum solute (ρ) in an electrolyte solution (ρ_{mob}). The system interacts with its periodic images (ρ', ρ'_{mob}).

Hence, one derives the chemical potentials as:

$$\mu_i^{\mathrm{pbc}} = k_{\mathrm{B}}T \ln \left[\frac{c_i^{\mathrm{bulk}} \Gamma V}{\int_V c^\circ \lambda(\mathbf{r}) \exp\left(-\frac{z_i \nu(\mathbf{r})}{k_{\mathrm{B}}T}\right) \mathrm{d}\mathbf{r}} \right], \; i = 1 \ldots p, \tag{25}$$

which is equivalent to:

$$\mu_i^{\mathrm{pbc}} = \underbrace{k_{\mathrm{B}}T \ln \frac{c_i^{\mathrm{bulk}}}{c^\circ}}_{\mu_i^{\mathrm{id}}} + \underbrace{k_{\mathrm{B}}T \ln \left(\frac{V\Gamma}{\int_V \lambda(\mathbf{r}) \exp\left(-\frac{z_i \nu(\mathbf{r})}{k_{\mathrm{B}}T}\right) \mathrm{d}\mathbf{r}} \right)}_{\mu_i^{\mathrm{ex}}}, \; i = 1 \ldots p, \tag{26}$$

where we have separated the ideal and excess components of the chemical potential (μ_i^{id} and μ_i^{ex}, respectively). The P-BE (Eq. 23) in PBCs has a solution only if the volume integral of the source term on RHS is zero. For an overall neutral electrolyte ($\sum_{i=1}^{p} z_i c_i^{\mathrm{bulk}} = 0$), this necessitates the volume integral of the quantum charge density to be also zero. This is ensured by introducing a compensating homogeneous background charge:

$$\rho^{\mathrm{pbc}}(\mathbf{r}) = \rho(\mathbf{r}) - \frac{\int_V \rho(\mathbf{r}) \, \mathrm{d}\mathbf{r}}{V}. \tag{27}$$

Substituting the expression for the chemical potential (μ_i^{pbc}) from Eq. 26 and the corrected charge density (ρ^{pbc}) from Eq. 27 into Eq. 23 gives the P-BE for PBC:

$$\nabla \cdot \left(\varepsilon(\mathbf{r}) \nabla \nu^{\mathrm{pbc}}(\mathbf{r}) \right) = -4\pi \left[\rho^{\mathrm{pbc}}(\mathbf{r}) + \sum_{i=1}^{p} z_i c_i^{\mathrm{bulk}} \lambda(\mathbf{r}) \exp\left(-\frac{z_i \nu^{\mathrm{pbc}}(\mathbf{r})}{k_{\mathrm{B}}T} + \frac{\mu_i^{\mathrm{ex}}}{k_{\mathrm{B}}T} \right) \right], \tag{28}$$

which can be solved for the electrostatic potential $\nu^{\mathrm{pbc}}(\mathbf{r})$ and the excess chemical potential μ_i^{ex} as defined in Eq. 26.

Substituting the expression for the chemical potential, μ_i^{pbc} (Eq. 26) and the electrostatic potential, ν^{pbc} found from Eq. 28 into the expression for concentrations (21) gives the

concentration of electrolyte species i in PBCs:

$$c_i^{\mathrm{pbc}}(\mathbf{r}) = c_i^{\mathrm{bulk}} \lambda(\mathbf{r}) \exp\left(-\frac{z_i \nu^{\mathrm{pbc}}(\mathbf{r})}{k_{\mathrm{B}}T} + \frac{\mu_i^{\mathrm{ex}}}{k_{\mathrm{B}}T}\right). \tag{29}$$

Substituting the chemical potentials (Eq. 26), electrostatic potential found from Eq. 28 and concentrations (Eq. 29) in the mean field free energy functional (Ω_{mf} in Eq. 5) gives the mean field free energy in PBCs:

$$\begin{aligned}
&\Omega_{\mathrm{mf}}^{\mathrm{pbc}}\left[\rho^{\mathrm{pbc}}(\mathbf{r}), \{c_i^{\mathrm{pbc}}(\mathbf{r})\}, \nu^{\mathrm{pbc}}(\mathbf{r})\right] \\
&= \int_V \left[\frac{1}{2}\rho^{\mathrm{pbc}}(\mathbf{r})\,\nu^{\mathrm{pbc}}(\mathbf{r}) - \frac{1}{2}\sum_{i=1}^{p} z_i c_i^{\mathrm{pbc}}(\mathbf{r})\,\nu^{\mathrm{pbc}}(\mathbf{r}) - k_{\mathrm{B}}T\sum_{i=1}^{p} c_i^{\mathrm{pbc}}(\mathbf{r})\right] \mathrm{d}\mathbf{r} \qquad (30) \\
&= \int_V \left[\frac{1}{2}\rho^{\mathrm{pbc}}(\mathbf{r})\,\nu^{\mathrm{pbc}}(\mathbf{r}) - \frac{1}{2}\sum_{i=1}^{p} z_i c_i^{\mathrm{pbc}}(\mathbf{r})\,\nu^{\mathrm{pbc}}(\mathbf{r})\right] \mathrm{d}\mathbf{r} - k_{\mathrm{B}}TV\Gamma\sum_{i=1}^{p} c_i^{\mathrm{bulk}}. \qquad (31)
\end{aligned}$$

B. Open Boundary Conditions (OBCs)

For a finite (bounded) solute in an infinite reservoir of electrolyte solution, as $\mathbf{r} \to \infty$, $\nu(\mathbf{r}) \to 0$, $V^{\mathrm{steric}}(\mathbf{r}) \to 0$, $\lambda(\mathbf{r}) \to 1$, $c_i(\mathbf{r}) \to c_i^{\mathrm{bulk}}$. Substituting this in Eq. 20 gives:

$$\mu_i^{\mathrm{obc}} = \mu_i^{\mathrm{id}} = k_{\mathrm{B}}T \ln\left(\frac{c_i^{\mathrm{bulk}}}{c^{\circ}}\right), \; i = 1 \ldots p. \tag{32}$$

Substituting the expression for μ_i^{obc} from Eq. 32 into Eq. 23 gives the P-BE in OBCs, which can be solved for the electrostatic potential:

$$\nabla \cdot \left(\varepsilon(\mathbf{r})\,\nabla\nu^{\mathrm{obc}}(\mathbf{r})\right) = -4\pi\left[\rho(\mathbf{r}) + \sum_{i=1}^{p} z_i c_i^{\mathrm{bulk}} \lambda(\mathbf{r}) \exp\left(-\frac{z_i \nu^{\mathrm{obc}}(\mathbf{r})}{k_{\mathrm{B}}T}\right)\right]. \tag{33}$$

Substituting the expression for the chemical potential, μ_i^{obc} (Eq. 26) and the electrostatic potential, ν^{obc} found from Eq. (33) into the expression for concentrations (21) gives the

concentration of electrolyte species i in OBCs:

$$c_i^{\mathrm{obc}}(\mathbf{r}) = c_i^{\mathrm{bulk}} \lambda(\mathbf{r}) \exp\left(-\frac{z_i \nu^{\mathrm{obc}}(\mathbf{r})}{k_{\mathrm{B}}T}\right),\ i = 1 \dots p, \tag{34}$$

which is the celebrated Boltzmann expression. Putting the chemical potentials (Eq. 32), electrostatic potential found from Eq. 33 and concentrations (Eq. 34) and the individual expressions back in the mean field free energy functional (Ω_{mf} in Eq. 5) gives the mean field free energy in OBCs:

$$\Omega_{\mathrm{mf}}^{\mathrm{obc}}\left[\rho(\mathbf{r}), \{c_i^{\mathrm{obc}}(\mathbf{r})\}, \nu^{\mathrm{obc}}(\mathbf{r})\right] = \int_V \left[\frac{1}{2}\rho(\mathbf{r})\,\nu^{\mathrm{obc}}(\mathbf{r}) - \frac{1}{2}\sum_{i=1}^{p} z_i c_i^{\mathrm{obc}}(\mathbf{r})\,\nu^{\mathrm{obc}}(\mathbf{r}) - k_{\mathrm{B}}T\sum_{i=1}^{p} c_i^{\mathrm{obc}}(\mathbf{r})\right] \mathrm{d}\mathbf{r}. \tag{35}$$

Linear Approximation for the Poisson-Boltzmann Equation

The linearized version of P-BE, Eq. 23, is much easier to solve numerically and is widely used in the literature. This approximation is formally valid if the electrostatic energy of ions is much smaller than the thermal energy, i.e. $\left|\frac{z_i \nu(\mathbf{r})}{k_{\mathrm{B}}T}\right| \ll 1$ for any $\mathbf{r}$. For monovalent electrolyte ions at room temperature the electrostatic potential should be much less than ~ 25 mV for the linear approximation to be valid.

In the case of PBCs we have to consider also the expansion of the excess chemical potential which enters in the concentration expression, see Eq. 29. We show in the Appendix that the linear approximation for the excess chemical potential is as follows:

$$\frac{\mu_i^{\mathrm{ex}}}{k_{\mathrm{B}}T} \approx \frac{z_i \bar{\nu}}{k_{\mathrm{B}}T},\ i = 1 \dots p, \tag{36}$$
$$\text{where } \bar{\nu} = \frac{1}{V\Gamma}\int_V \lambda(\mathbf{r})\nu(\mathbf{r})\mathrm{d}\mathbf{r}\ .$$

Now we can expand the exponential in Eq. 29 to first order and we obtain the following form

for the linearized P-BE:

$$\nabla \cdot (\varepsilon(\mathbf{r})\, \nabla\nu(\mathbf{r})) - l_{\mathrm{D}}^{-2}\lambda(\mathbf{r})\, (\nu(\mathbf{r}) - \bar{\nu}) = -4\pi\rho^{\mathrm{pbc}}(\mathbf{r}) \ , \tag{37}$$

where

$$l_{\mathrm{D}} = \left(\frac{k_{\mathrm{B}}T}{4\pi \sum_{i=1}^{p} z_i^2 c_i^{\mathrm{bulk}}} \right)^{1/2} \tag{38}$$

is the Debye length. We note that the definition of $\bar{\nu}$ implies that $\int_V \lambda(\mathbf{r})\, (\nu(\mathbf{r}) - \bar{\nu}) \mathrm{d}\mathbf{r} = 0$ which makes Eq. 37 consistent with PBCs.

The electrostatic potential shift $\bar{\nu}$ can be absorbed in $\nu(\mathbf{r})$ by redefining $\nu(\mathbf{r}) \to \nu(\mathbf{r}) + \bar{\nu}$ and we obtain the standard definition of linearized P-BE:

$$\nabla \cdot (\varepsilon(\mathbf{r})\, \nabla\nu(\mathbf{r})) - l_{\mathrm{D}}^{-2}\lambda(\mathbf{r})\, \nu(\mathbf{r}) = -4\pi\rho^{\mathrm{pbc}}(\mathbf{r}) \, , \tag{39}$$

which is valid also for OBCs. In the case of PBCs one has to keep in mind that the solution of the previous equation must satisfy the condition $\int_V \lambda(\mathbf{r})\, \nu(\mathbf{r})\, \mathrm{d}\mathbf{r} = 0$. All other quantities (e.g. grand potential, electrolyte concentrations, etc.) can be obtained by using the potential from the linearized P-BE in the expressions we have derived already.

Solvation Energies

Solvation energies are defined as:[29,40]

$$\begin{aligned} \Delta\Omega &= \Omega - \Omega_{\mathrm{vac}} - \Omega_{\mathrm{electrolyte}} && (40) \\ &= \Omega\left[\rho(\mathbf{r}) \, , \{c_i(\mathbf{r})\}, \nu(\mathbf{r})\right] && (41) \\ &- \Omega\left[\rho_{\mathrm{vac}}(\mathbf{r}) \, , \{c_i(\mathbf{r})\} = 0, \nu_{\mathrm{vac}}(\mathbf{r})\right] \\ &- \Omega\left[\rho(\mathbf{r}) = 0, \{c_i(\mathbf{r})\} = \{c_i^{\mathrm{bulk}}\}, \nu(\mathbf{r}) = 0\right] , \end{aligned}$$

where the respective terms are the total free energy of the solute in the electrolyte solution, the total free energy of the solute in vacuum, and the total free energy of the pure electrolyte. The energy of the pure electrolyte in PBCs, under the assumption that the electrolyte anions and cations are uniformly distributed making the total electrolyte charge density zero, can be obtained by substituting $\rho^{\mathrm{pbc}}_{\mathrm{electrolyte}}(\mathbf{r}) = 0$, $\{c_i(\mathbf{r})\}_{\mathrm{electrolyte}} = \{c_i^{\mathrm{bulk}}\}$, $\nu_{\mathrm{electrolyte}}(\mathbf{r}) = 0$, ($\Gamma_{\mathrm{electrolyte}} = 1$) in the expression for free energy in Eq. 30:

$$\Omega^{\mathrm{pbc}}_{\mathrm{electrolyte}} = \Omega^{\mathrm{pbc}}_{\mathrm{mf}}\left[\rho(\mathbf{r}) = 0, \{c_i(\mathbf{r})\} = \{c_i^{\mathrm{bulk}}\}, \nu(\mathbf{r}) = 0\right] = -k_{\mathrm{B}}TV\sum_{i=1}^{p} c_i^{\mathrm{bulk}}\,, \tag{42}$$

and the mean-field solvation energies can be written as:

$$\Delta\Omega^{\mathrm{pbc}}_{\mathrm{mf}} = \int_V \left[\frac{1}{2}\rho^{\mathrm{pbc}}(\mathbf{r})\,\nu^{\mathrm{pbc}}(\mathbf{r}) - \frac{1}{2}\rho^{\mathrm{pbc}}_{\mathrm{vac}}(\mathbf{r})\,\nu^{\mathrm{pbc}}_{\mathrm{vac}}(\mathbf{r}) - \frac{1}{2}\sum_{i=1}^{p} z_i c_i^{\mathrm{pbc}}(\mathbf{r})\,\nu^{\mathrm{pbc}}(\mathbf{r})\right]\mathrm{d}\mathbf{r} + k_{\mathrm{B}}T\,(1-\Gamma)\,V\sum_{i=1}^{p} c_i^{\mathrm{bulk}}. \tag{43}$$

Similarly in OBCs, the energy of the pure electrolyte can be obtained by substituting $\rho_{\mathrm{electrolyte}}(\mathbf{r}) = 0, \{c_i(\mathbf{r})\}_{\mathrm{electrolyte}} = \{c_i^{\mathrm{bulk}}\}, \nu_{\mathrm{electrolyte}}(\mathbf{r}) = 0$ in the expression for free energy (Eq. 35):

$$\Omega^{\mathrm{obc}}_{\mathrm{electrolyte}} = \Omega^{\mathrm{obc}}_{\mathrm{mf}}\left[\rho(\mathbf{r}) = 0, \{c_i(\mathbf{r})\} = \{c_i^{\mathrm{bulk}}\}, \nu(\mathbf{r}) = 0\right] = -k_{\mathrm{B}}TV\sum_{i=1}^{p} c_i^{\mathrm{bulk}}, \tag{44}$$

and the mean field component of the solvation energy can be written as:

$$\Delta\Omega^{\mathrm{obc}}_{\mathrm{mf}} = \int_V \left[\frac{1}{2}\rho(\mathbf{r})\,\nu^{\mathrm{obc}}(\mathbf{r}) - \frac{1}{2}\rho_{\mathrm{vac}}(\mathbf{r})\,\nu^{\mathrm{obc}}_{\mathrm{vac}}(\mathbf{r}) - \frac{1}{2}\sum_{i=1}^{p} z_i c_i^{\mathrm{obc}}(\mathbf{r})\,\nu^{\mathrm{obc}}(\mathbf{r}) + k_{\mathrm{B}}T\sum_{i=1}^{p}\left(c_i^{\mathrm{bulk}} - c_i^{\mathrm{obc}}(\mathbf{r})\right)\right]\mathrm{d}\mathbf{r}. \tag{45}$$

We should note here that the above equations for the solvation free energies do not assume that the same solute structure is used in vacuum and in electrolyte solution. Therefore they are valid also in the case when the structure of the solute has been relaxed separately in vacuum and in solution.

Electrolyte effect on Solvation Energies

It is useful to describe the electrolyte effect on solvation energies as the difference of solvation energy in electrolyte at $\{c_i^{\text{bulk}}\}$ and solvation energy in pure solvent at $\{c_i^{\text{bulk}} = 0\}$:

$$\Delta\Delta\Omega = \Delta\Omega\left[\{c_i^{\text{bulk}}\}\right] - \Delta\Omega\left[\{c_i^{\text{bulk}} = 0\}\right] \tag{46}$$

$$= \Omega - \Omega_{\text{sol}} - \Omega_{\text{electrolyte}}, \tag{47}$$

where the respective terms are the total free energy of the solute in the electrolyte solution $\{c_i^{\text{bulk}}\}$, the total free energy of the solute in pure solvent $\{c_i^{\text{bulk}} = 0\}$ and the total free energy of the pure electrolyte. The mean field component in PBCs is:

$$\Delta\Delta\Omega_{\text{mf}}^{\text{pbc}} = \int_V \left[\frac{1}{2}\rho^{\text{pbc}}(\mathbf{r})\,\nu^{\text{pbc}}(\mathbf{r}) - \frac{1}{2}\rho_{\text{sol}}^{\text{pbc}}(\mathbf{r})\,\nu_{\text{sol}}^{\text{pbc}}(\mathbf{r}) - \frac{1}{2}\sum_{i=1}^{p} z_i c_i^{\text{pbc}}(\mathbf{r})\,\nu^{\text{pbc}}(\mathbf{r})\right] \mathrm{d}\mathbf{r} + k_{\text{B}}T\,(1-\Gamma)\,V\sum_{i=1}^{p} c_i^{\text{bulk}}, \tag{48}$$

and in OBCs it is:

$$\Delta\Delta\Omega_{\text{mf}}^{\text{obc}} = \int_V \left[\frac{1}{2}\rho(\mathbf{r})\,\nu^{\text{obc}}(\mathbf{r}) - \frac{1}{2}\rho_{\text{sol}}(\mathbf{r})\,\nu_{\text{sol}}^{\text{obc}}(\mathbf{r}) - \frac{1}{2}\sum_{i=1}^{p} z_i c_i^{\text{obc}}(\mathbf{r})\,\nu^{\text{obc}}(\mathbf{r}) + k_{\text{B}}T\sum_{i=1}^{p}\left(c_i^{\text{bulk}} - c_i^{\text{obc}}(\mathbf{r})\right)\right] \mathrm{d}\mathbf{r}. \tag{49}$$

Activity Coefficients

The behavior of non-ideal electrolytes can be described by their activity coefficients.[44] We follow the approach described by Ringe *et al.* to compute activity coefficients.[29] We consider an electrolyte solution (for example "continuum" $LiPF_6$) at concentration $\{c_i^{\text{bulk}}\}$. We add a molecule of quantum solute j (for example "quantum" PF_6^-) to this solution. The chemical potential of the quantum solute j can then be given by:

$$\mu_j\left[\{c_i^{\text{bulk}}\}\right] = \mu_j\left[\{c_i^{\text{bulk}} = 0\}\right] + k_{\text{B}}T\ln\gamma_j, \tag{50}$$

where γ_j is the activity coefficient of the solute j at electrolyte concentration $\{c_i^{\text{bulk}}\}$. The chemical potential of the quantum solute j represents the change in the free energy per number of molecules (n_j) of solute j:

$$\left.\frac{\partial \Omega}{\partial n_j}\right|_{\{c_i^{\text{bulk}}\}} = \left.\frac{\partial \Omega}{\partial n_j}\right|_{\{c_i^{\text{bulk}}=0\}} + k_{\text{B}}T \ln \gamma_j, \tag{51}$$

which can be written in terms of solvation energies because the energies of solute j in vacuum cancel out:

$$\Delta\Omega\left[\{c_i^{\text{bulk}}\}\right] - \Delta\Omega\left[\{c_i^{\text{bulk}} = 0\}\right] = k_{\text{B}}T \ln \gamma_j, \tag{52}$$

or, equivalently

$$\frac{\Delta\Delta\Omega\left[\{c_i^{\text{bulk}}\}\right]}{k_{\text{B}}T} = \ln \gamma_j. \tag{53}$$

Hence, activity coefficients can be computed from the electrolyte effect on solvation energies ($\Delta\Delta\Omega$), which is described in the previous section. The mean activity coefficient of q solutes (for example Li^+ and PF_6^-) is calculated as:

$$\ln \gamma_{\text{mean}} = \frac{1}{q}\sum_{j=1}^{q} \ln \gamma_j. \tag{54}$$

Implementation

The electrostatic potential $\nu(\mathbf{r})$ is computed with the P-BE solver DL_MG[17,45] for Eq. 23. In the case of PBCs, DL_MG computes also the excess chemical potential. The following details of the solution process are worth knowing in this case. One can see that Eq. 21 is invariant under the following transformations:

$$\nu(\mathbf{r}) \to \nu(\mathbf{r}) + \text{C} \tag{55}$$

$$\mu_i \to \mu_i + z_i \text{ C}, \tag{56}$$

where C is an arbitrary constant. The solver's algorithm subtracts the average electrostatic potential defined by

$$\bar{\nu} = \frac{1}{V\Gamma} \int_V \lambda(\mathbf{r})\, \nu(\mathbf{r})\, \mathrm{d}\mathbf{r} \tag{57}$$

from the approximate solution in every iteration of the Newton solver. This implies that the solution satisfies the the following condition:

$$\int_V \lambda(\mathbf{r})\, \nu(\mathbf{r})\, \mathrm{d}\mathbf{r} = 0\ . \tag{58}$$

The choice for the potential shift fixes the value of the excess chemical potential. The same shift is applied to the solution of the linearized P-BE with PBCs.

The electronic structure is found with the ONETEP linear-scaling DFT program. Kohn-Sham DFT is reformulated in terms of single particle density matrix:[4]

$$\rho_{\mathrm{e}}(\mathbf{r}, \mathbf{r}') = \phi_\alpha(\mathbf{r})\, K^{\alpha\beta} \phi^*_\beta(\mathbf{r}'), \tag{59}$$

where the matrix $\mathbf{K}$ is the 'density kernel' and the localized orbitals $\{\phi_\alpha\}$ are Non-orthogonal Generalized Wannier Functions (NGWFs).[42] The summation is implied over repeated Greek indices α and β. The NGWFs and the density kernel are self-consistently optimised during the calculation. The NGWFs are expanded in a basis set of periodic sinc (psinc) functions[42,46] which are equivalent to a plane wave basis set and whose quality is controlled by a single kinetic energy cutoff parameter, as in plane waves. Within this formalism, the kinetic energy can be written as:

$$T_{\mathrm{s}}\left[\rho_{\mathrm{e}}\right] \equiv T_{\mathrm{s}}\left[\{\phi_\alpha\}, \mathbf{K}\right] = K^{\alpha\beta} \left\langle \phi_\beta \left| -\frac{1}{2}\nabla^2 \right| \phi_\alpha \right\rangle . \tag{60}$$

The contribution due to the pseudopotentials can be written as:

$$V_{\mathrm{ps}}\left[\rho_{\mathrm{e}}\right] \equiv V_{\mathrm{ps}}\left[\{\phi_\alpha\}, \mathbf{K}\right] = K^{\alpha\beta} \left\langle \phi_\beta \left| \nu_{\mathrm{ps}} \right| \phi_\alpha \right\rangle = K^{\alpha\beta} \left\langle \phi_\beta \left| \nu_{\mathrm{ps,l}} \right| \phi_\alpha \right\rangle + K^{\alpha\beta} \left\langle \phi_\beta \left| \nu_{\mathrm{ps,nl}} \right| \phi_\alpha \right\rangle , \tag{61}$$

where the subscripts 'l' and 'nl' represent the local pseudopotential and the non-local part of the pseudopotential in the Kleinman and Bylander representation. The electronic component of the electrostatic energy (U^{elec}) in Eq. 6 can be written as:

$$\int \rho_{\text{e}}(\mathbf{r})\,\nu(\mathbf{r})\,\mathrm{d}\mathbf{r} = K^{\alpha\beta}\,\langle\phi_\beta\,|\nu|\,\phi_\alpha\rangle\,. \tag{62}$$

The total free energy is minimized with respect to the density kernel $\mathbf{K}$ and the NGWFs $\{\phi_\alpha\}$ to obtain the ground state of the system as shown schematically in Figure 2.

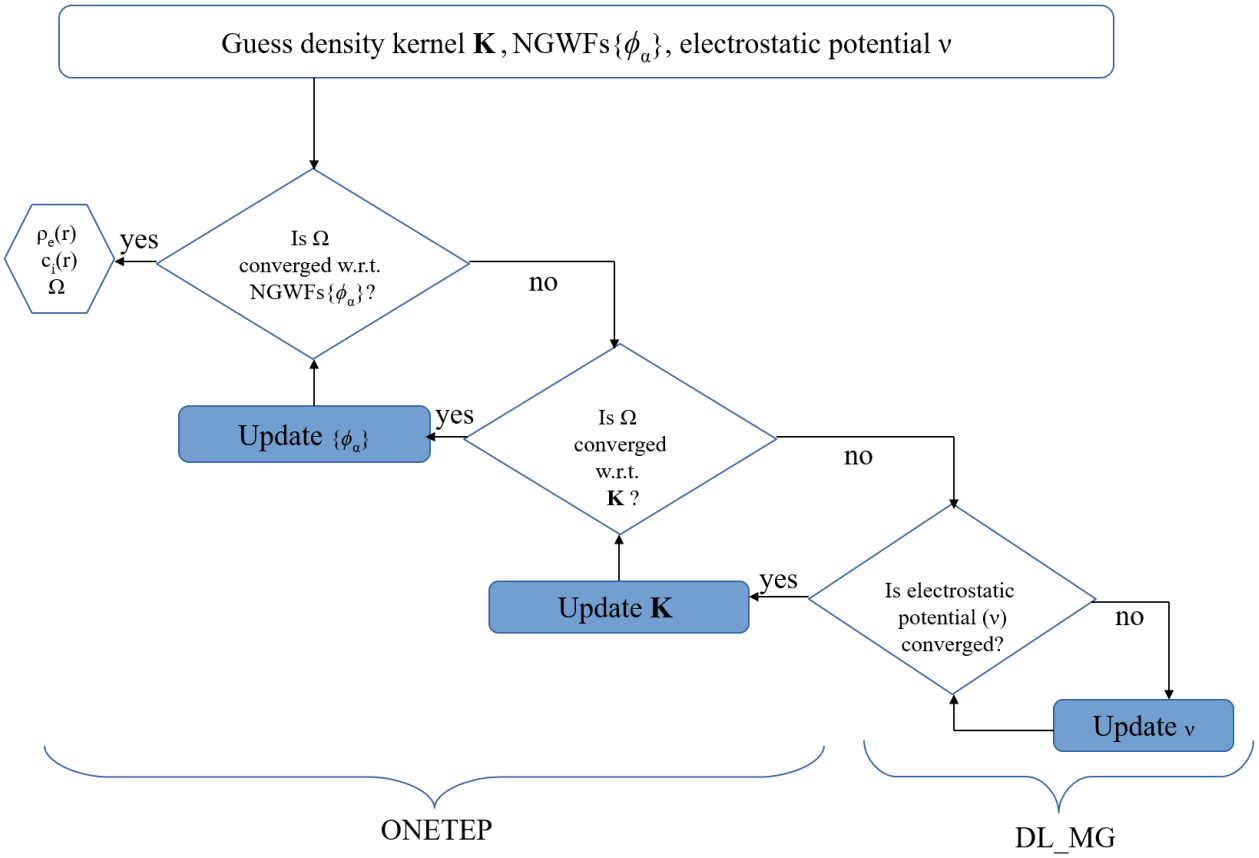

Figure 2: Solution procedure for the electronic problem inside ONETEP and electrostatic problem inside DL_MG.

In ONETEP the quantities of interest ($\rho(\mathbf{r})$, $\nu(\mathbf{r})$, $\varepsilon(\mathbf{r})$, $\lambda(\mathbf{r})$, $c_i(\mathbf{r})$) are represented on a Cartesian grid, with a typical spacing of 0.4-0.5 a_0. On the same Cartesian grid, the ionic cores of charges $\{Z_i\}$ are represented by smeared Gaussians, with a smearing width (σ_i) of

$0.8\,a_0$ as per our previous work:[22]

$$\rho_{\mathrm{nuc}}(\mathbf{r}) = \sum_{i}^{\mathrm{N_{atoms}}} \frac{Z_i}{\left(\sigma_i\sqrt{\pi}\right)^3} e^{-\left(\frac{|\mathbf{r}-\mathbf{R}_i|}{\sigma_i}\right)^2}. \tag{63}$$

This is done to facilitate the handling of the core charges in DL_MG, which cannot directly deal with point charges. The effect of this modification is subtracted out in the final energy expression (cf. Ref. 22, Appendix A).

Several implementation details differ depending on the choice of boundary conditions (BCs). Table 1 summarizes the relevant changes.

Table 1: Summary of implementation differences depending on the choice of BCs.

Implementation detail	OBCs	PBCs
Core-core interaction in the solute.	Direct Coulombic sum of pairwise interactions, see Ref. 43, eq. (8).	Ewald sum, with neutralizing background charge if the solute is not charge-neutral.
Local pseudopotential in the solute.	Generated in real space as a sum of spherically symmetrical contributions from solute atomic cores, see Ref. 43, eq. (B4).	Generated in reciprocal space, see Ref. 47, eq. (6.21).
Boundary conditions for $\nu(\mathbf{r})$ passed to the multigrid solver.	Dirichlet BCs calculated according to Ref. 22, eq. (4) (in vacuum); Ref. 22, eq. (5) (in solvent in the absence of electrolyte); Ref. 22, eq. (5) with Debye screening (in solvent when the electrolyte is present).	No explicit Dirichlet BCs, only a continuity condition on simulation box faces.
Interaction between the smeared ions in the solute, see Ref. 22, Appendix A.	Calculated in real space, according to Ref. 22, eq. (A11).	Densities calculated in real space, according to Ref. 22, eq. (A1), using the minimum image convention (MIC) for periodicity. Periodic potential calculated in reciprocal space (see Ref. 48, Sec. 4.3).
Calculation of $\nabla\rho_{\mathrm{e}}$, needed for determining the surface area of the solute cavity.	Calculated in real space using high-order finite differences.	Calculated in reciprocal space using FFTs.

Results and Discussions

To test and demonstrate some of the capabilities of our method we present two exemplar applications: determination of mean activity coefficients (which are performed with calculations in OBCs) and simulations of a graphite interface with electrolyte solution and its effect on intercalated Li (calculations performed in PBCs). In all calculations we have used the PBE exchange-correlation functional, an 1000 eV kinetic energy cut-off for the psinc basis set, and 8.0 a_0 radii for the NGWFs.

A. Activity Coefficients

The model contains two parameters: the isovalue of solute electronic density ($\rho_{\mathrm{e}}^{\lambda}$) and the solvent radius (R_k^{solvent}), in the description of the accessibility function, which need to be determined by calibrating against a measurable experimental quantity. For this purpose we use the mean activity coefficients of electrolytes that are sensitive to electrolyte concentrations and have been used to calibrate the unknown parameters in the description of the accessibility function.[29] Experimental mean activity coefficients are available for a large set of electrolytes in aqueous,[49] and organic solvents.[50] To calculate the activity coefficients, we place a single molecule of cation/anion at the center of a simulation cell with sides 20Å × 20Å × 20Å and calculate the electrolyte effect on solvation free energies ($\Delta\Delta\Omega$) as a function of the electrolyte concentration (c_i^{bulk}). The mean activity coefficient is then calculated using equations (53) and (54). We consider two systems: electrolytes in aqueous and non-aqueous solvents which show negative and positive deviations from ideal solutions.

Aqueous Solvents: KCl in water

The standard bulk permittivity of water (78.54) and surface tension (0.07415 N/m) at 298 K are used in our solvent model. We set the solvent radius ($R_k^{\mathrm{solvent}} \approx 2.0\ a_0$) approximately as the size of a water molecule, and vary the isovalue of solute electronic density ($\rho_{\mathrm{e}}^{\lambda}$) to match

the experimental activity coefficients. We show plots of computed activity coefficients with respect to the square root of electrolyte concentration in Figure 3 along with experimental values from literature,[49] and a computational study by Ringe *et al.*[29] We see reasonable prediction of activity coefficients when using the non-linearised P-BE for different values of solute electronic density (ρ_e^λ). Further, we show the results obtained from the linearized P-BE. In this case, by reducing the solvent radius we approach the behavior of point charge electrolytes, as in Debye-Hückel theory.[51]

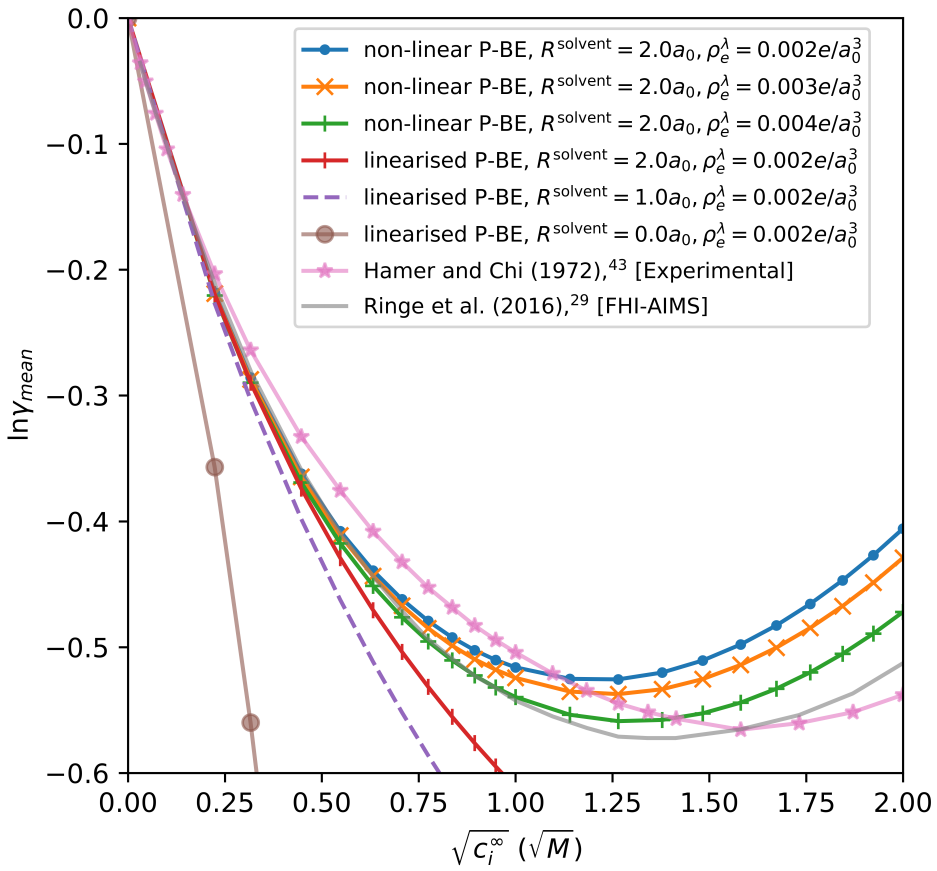

Figure 3: Mean activity coefficients for KCl in water at 298 K as a function of concentration and for different values of the atomic electronic density isovalue parameter ρ_e^λ which determines the extent of the accessibility function. Calculations with the linearized approximation to P-BE are also shown.

Non-Aqueous Solvents: $LiPF_6$ in Ethylene Carbonate

The experimental values of bulk permittivity of ethylene carbonate (EC) ($\varepsilon_{\text{bulk}} = 90.7$)[52] and surface tension of EC (0.0506 N/m),[53] are taken from the literature. In this case we set the solvent radius to be $R_k^{\text{solvent}} = 10.5\ a_0$ to approximate the size of an EC molecule, and we vary the isovalue of solute electronic density ($\rho_{\text{e}}^{\lambda}$) to match the experimental activity coefficients. We note here that the EC molecule is not spherical and solvent radius represents an effective radius of solvation shell around electrolyte ions, that is formed by EC molecules. The solvent radius required in the case of $LiPF_6$/EC system (10.5 a_0) is substantially larger than that required for aqueous KCl (2 a_0), due to the large solvation radius of $Li^+(EC)_4$ clusters found in the solution,[54,55] which prevents the electrolyte ions from coming close to the solute. We show the plot of the computed activity coefficients as a function of the square root of electrolyte concentration in Figure 4 along with experimental values from literature.[50] We see a good match for $\rho_{\text{e}}^{\lambda} = 0.002\ e/a_0^3$. Further, we observe that we need similar values of solute electronic density ($\rho_{\text{e}}^{\lambda}$) of around 0.002-0.003 e/a_0^3 to fit the experimental activity coefficients of electrolytes in both aqueous and non-aqueous solvents. This suggests a degree of transferability of this parameter. We also plot lines from the linearized approximation of P-BE where we reduce the solvent radius to show the behavior of point charges from the Debye-Hückel theory.[51]

As a final comment for the calculations of the mean activity coefficients, we should note that while they do not perfectly reproduce the experimental results, they can provide additional insights, such as the activity coefficients of the individual ions, from which we obtain the average activity coefficients, that we present here and are measured in experiments. For example, Cl^- is much bigger (in terms of excluded volume) and more polarisable than K^+, with similar considerations about $LiPF_6$. In our model the different ions do have different radii as these are determined by the density isovalue of $\rho_{\text{e}}^{\lambda}$ which will produce different accessibility radii depending on the extent of the electronic density of each atom or ion.

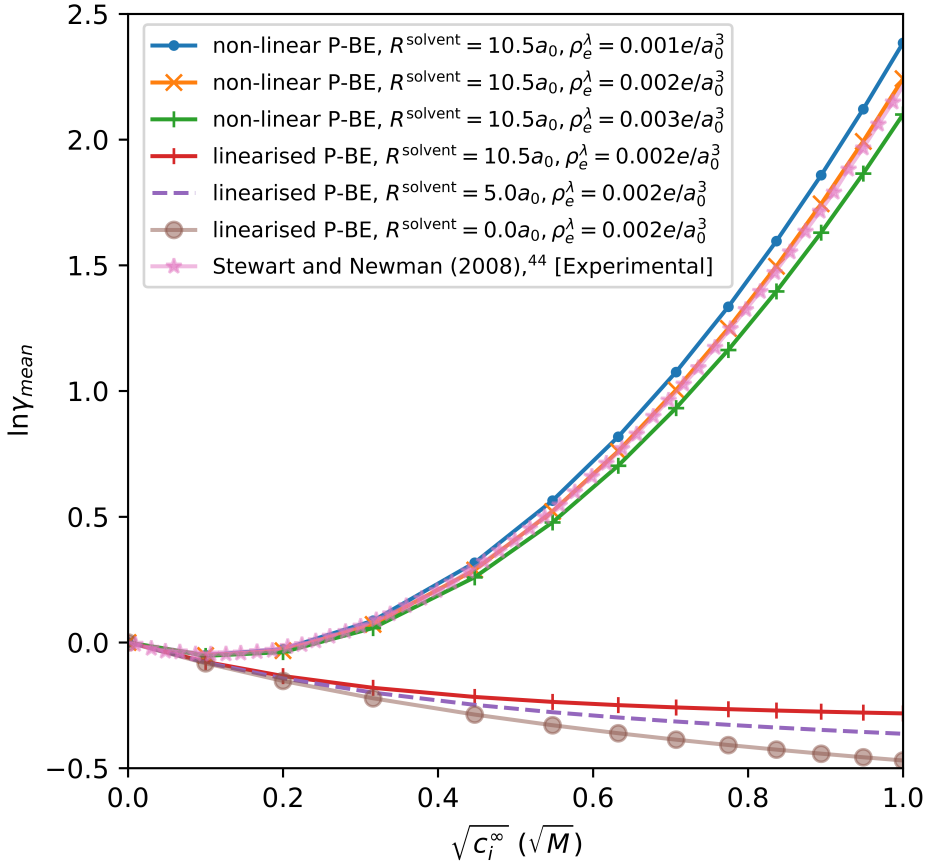

Figure 4: Mean activity coefficients for $LiPF_6$ in ethylene carbonate at 308 K as a function of concentration and for different values of the atomic electronic density isovalue parameter ρ_e^λ which determines the extent of the accessibility function. Calculations with the linearized approximation to P-BE are also shown.

B. Solid-electrolyte interfaces: Li-graphite slab in contact with $LiPF_6$ electrolyte in ethylene carbonate (EC) solvent

Finally, in order to demonstrate the capability of our electrolyte model in PBCs we present a calculation on an interface between a dilute lithiated graphite slab and a solution containing electrolyte. This can be considered as a very simplified model of the anode in contact with the electrolyte solution in a Li-ion battery, in an almost fully discharged state. The system we simulate consists of a 1634-atom hydrogen-terminated periodic graphite slab with two Li atoms ($Li_2C_{1440}H_{192}$) in $LiPF_6$ electrolyte at $c_i^{\text{bulk}} = 0.5$ M. The graphite layers are on top of each other (AA stacking) to represent a simplified metastable geometry rather than the more complicated stackings that can occur during the charging and discharging of a Li-ion battery. The simulation cell is orthorhombic with sides of $27.526\text{Å} \times 25.605\text{Å} \times 62.247\text{Å}$. The graphite slab is periodic in x and y directions and is placed in the middle of the simulation cell in the z direction. We have optimized the geometry of the slab in vacuum. We have implemented the force terms in ONETEP for geometry optimization in pure solvent. We do not know if there are additional force terms due to the electrolyte solution that would need to be taken care during geometry optimization. We plan to study it in future.

A Li atom is placed symmetrically on the bottom and top surfaces of the slab, thereby eliminating any periodic dipole interaction artifacts. As the interfaces with the electrolyte are symmetric on both sides the grand potential (Ω) will describe the energetics of both identical interfaces. We assume the solvent in our model to be ethylene carbonate (EC) and we use the bulk permittivity of ethylene carbonate (EC) ($\varepsilon_{\text{bulk}} = 90.7$)[52] and surface tension of EC (0.0506 N/m),[53] which are taken from the literature. The parameters for the accessibility radius are taken as estimated from the calibration of activity coefficients in the previous section. The solute isodensity parameter, which represents the solute size is taken to be $\rho_e^{\lambda} = 0.001\, e/a_0^3$, and the solvent radii for each element are set to $R_{\text{H}}^{\text{solvent}} = 3.0\, a_0$, $R_{\text{C}}^{\text{solvent}} = 3.0\, a_0$, $R_{\text{Li}}^{\text{solvent}} = 0.0\, a_0$ (Li inside the graphite edge is desolvated). The total accessible volume is $V_{\text{acc}} = 178993.3338\ a_0^3$ and the total number of each type of electrolyte ions,

$N_i = c_i^{\text{bulk}} V_{\text{acc}} = 7.9866$. In Figure 5(a) we show plots of electrolyte concentration isovalue surfaces for this system at concentrations $c_{\text{Li}^+}(\mathbf{r}) = 0.504$ M and $c_{\text{PF}_6^-}(\mathbf{r}) = 0.504$ M in red and blue respectively. These values are chosen to be higher than the bulk concentration in order to demonstrate the local variation in concentration close to the charged species, in this case showing the region with excess electrolyte concentration, $c_{\text{ex}}(\mathbf{r}) \equiv c_i(\mathbf{r}) - c_i^{\text{bulk}} = 0.004$ M. We see that, as expected, the Li at the graphite surface attracts the negative electrolyte ions (blue) closer to itself, while the positive electrolyte (red) concentrates close to the surface carbon atoms that are not in the vicinity of the intercalated Li. The Mulliken charge on Li is positive (+1.58 e), which explains the accumulation of negative electrolyte near Li. This is possible as the PAWs used for Li have 3 valence electrons and can lose more than one electron charge.

We also consider the case where Li is well outside the graphite slab as shown in Figure 5(b). For this case, $R_{\text{Li}}^{\text{solvent}} = 10.0\ a_0$ to represent the fact that the Li is solvated by a solvation shell of EC solvent (as found from calibration of activity coefficients in previous section). The total accessible volume is $V_{\text{acc}} = 158346.3032\ a_0^3$ and the total number of each type of electrolyte ions, $N_i = c_i^{\text{bulk}} V_{\text{acc}} = 7.0653$. Here again, each Li atom attracts the negative electrolyte ions (blue) closer to itself, while the positive electrolyte (red) concentrates close to the surface carbon atoms. The Mulliken charge on Li is positive (1.00 e) Hence, the presence of Li causes a polarisation of the electrolyte system.

The electrostatic potential in a plane containing the Li atoms that is parallel to the graphite planes is shown in Figure 6 for both the cases. Positive potential builds up around the Li atoms, which transitions to negative potential in the region near the carbon atoms. The white area shows regions of zero potential. The reference potential has been set according to equation (58).

The difference in free energies of the systems with Li at the edge (a) and in the electrolyte (b) is $\Omega_{(a)} - \Omega_{(b)} = -2.34$ eV, which suggests higher stability of the Li at the graphite edge rather than in the electrolyte. The same difference in vacuum is -5.70 eV. In vacuum, the Li

outside the graphite slab is unsolvated which makes it highly unstable, leading to a larger difference in the free energies. In pure solvent (i.e. $c_i^{\text{bulk}} = 0$), the same difference is -2.30 eV as compared to -2.34 eV in presence of electrolyte at $c_i^{\text{bulk}} = 0.5$M. This is suprising at first as one would expect the Li outside the graphite to be more stable in electrolyte than in pure solvent . However, there is significant stabilisation of the Li inside the graphite as well, due to the surface charge of the interface which attracts both positive and negative electrolyte. Hence this delicate balance would need to be investigated in more detail, also as a as a function of concentration of electrolyte (c_i^{bulk}), but in this case the addition of $c_i^{\text{bulk}} = 0.5$M electrolyte stabilizes the Li at the graphite edge by about 0.04 eV with respect to the pure solvent case.

A more detailed study of this system is beyond the scope of this paper.Taking advantage of the unique capabilities of ONETEP for large-scale calculations, where graphite systems with up to 10,000 atoms can be routinely studied, and the methodology described here, we aim to construct more complex and realistic models of graphite interfaces, building up to an atomistic model of the Solid-Electrolyte-Interphase (SEI). We anticipate that such calculations will provide detailed information about the interfacial intercalation kinetics as a function of electrolyte concentration and potential (state of charge).

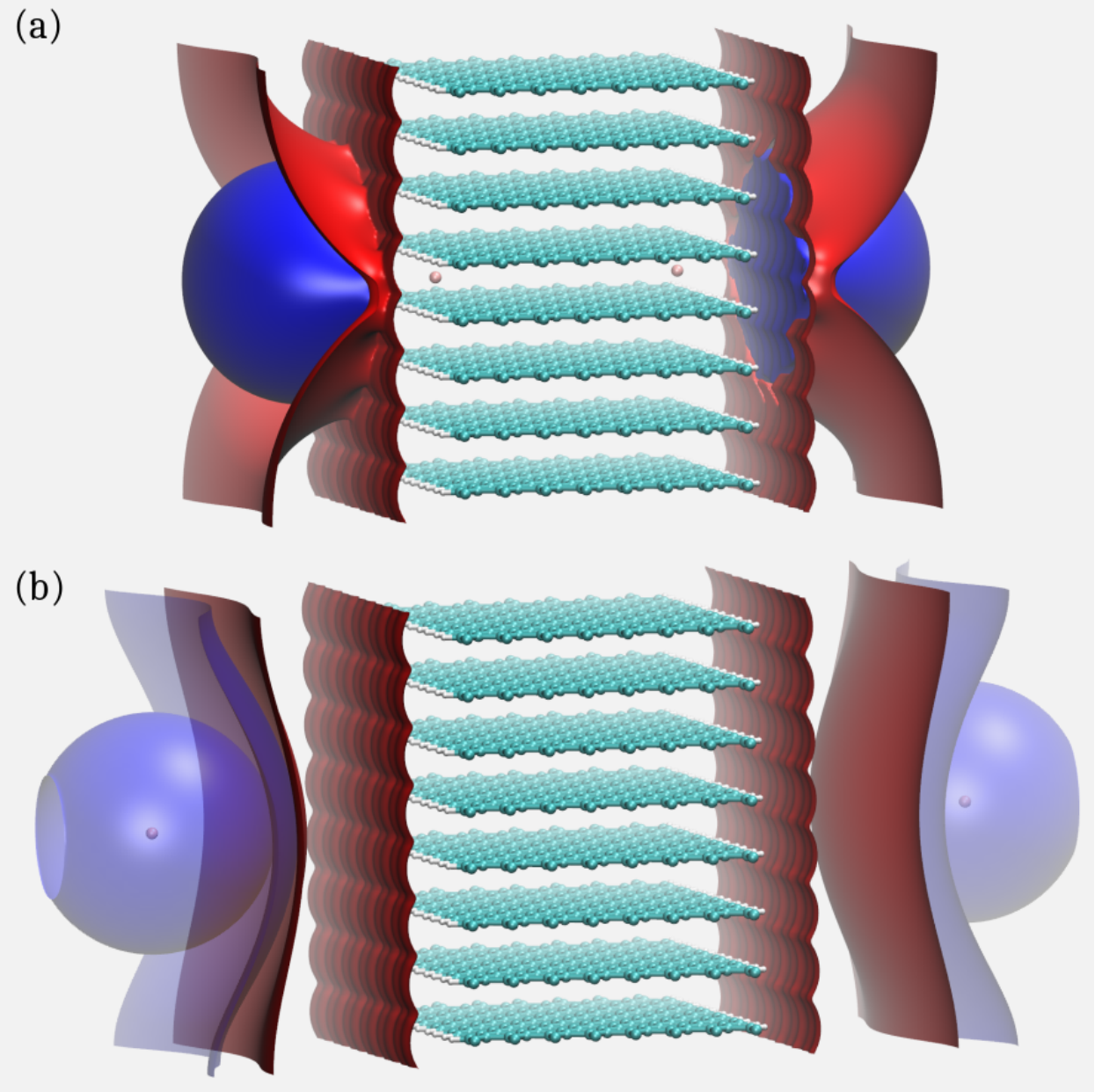

Figure 5: The electrolyte concentration isovalue surfaces, $c_{Li^+} = 0.504$M (red) and $c_{PF_6^-} = 0.504$M (blue) for the Li-graphite system with 1634 atoms ($Li_2C_{1440}H_{192}$). (a) Li is at graphite edge. (b) Li is in electrolyte. The VMD software has been used to plot the image.[56]

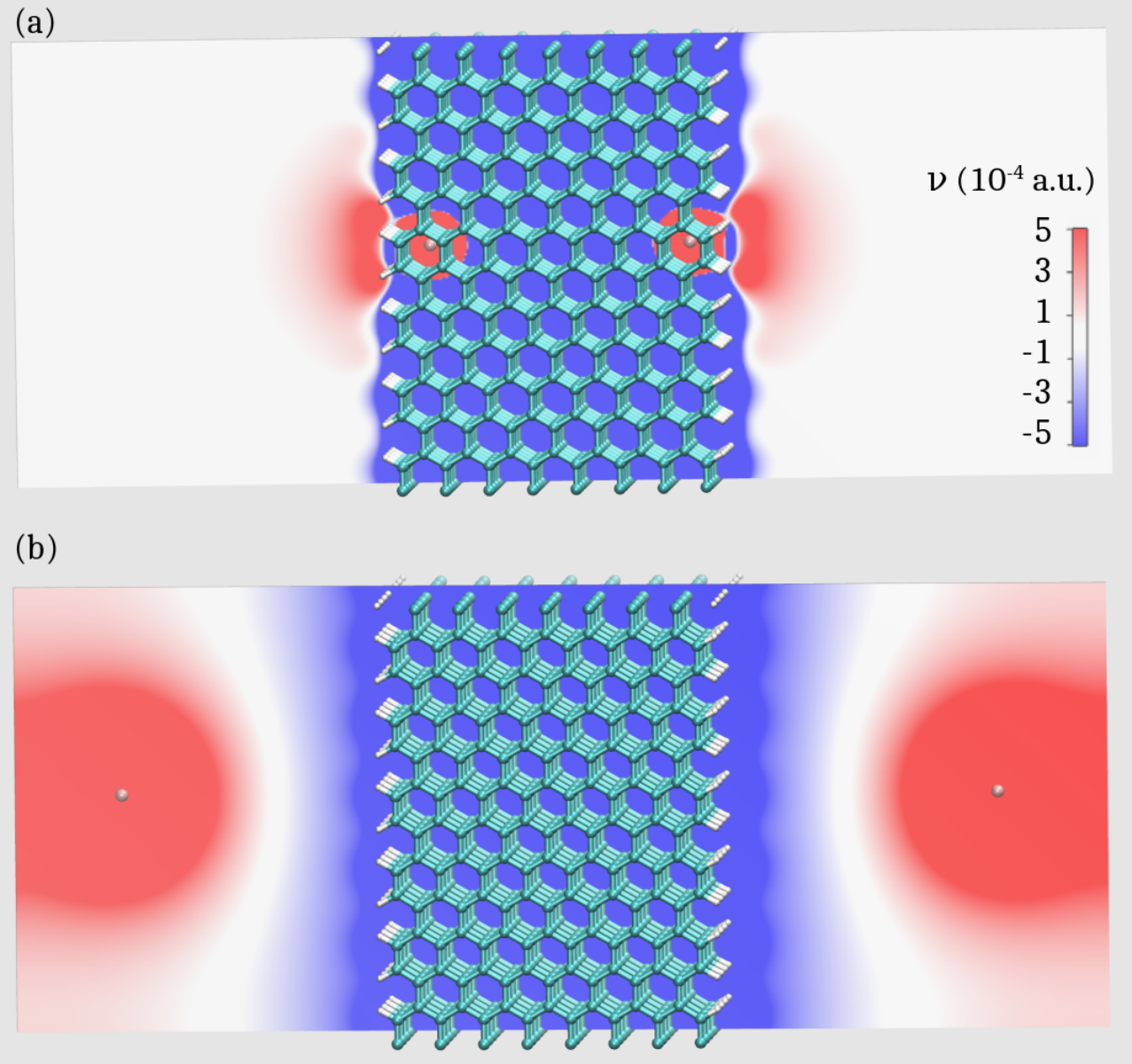

Figure 6: Electrostatic potential (ν) contours on the plane containing the two Li ions shown for the Li-graphite system with 1634 atoms ($Li_2C_{1440}H_{192}$). (a) Li at the graphite edge. (b) Li in the electrolyte. The VMD software has been used to plot the image.[56]

Conclusions

We have presented the implementation of a hybrid continuum-atomistic model for including the effects of surrounding electrolyte in Density Functional Theory (DFT) calculations. The model is implemented within the ONETEP linear-scaling DFT code which allows calculations with much larger numbers of atoms than conventional DFT. The concentration of electrolyte ions is described as a scalar field surrounding the quantum solute and the solvent is a polarisable dielectric continuum medium. The model extends our previous minimal-parameter solvent-only model in ONETEP, where the solute cavity was determined by isovalue surfaces of the electronic density. In order to describe in a consistent way the entire solute-solvent-electrolyte system we have developed a grand canonical functional incorporating the electron kinetic and exchange correlation energies, the total electrostatic energy, entropy and chemical potentials of surrounding electrolyte, osmotic pressure, and the effects of cavitation, dispersion and repulsion. The DFT calculation is performed fully self-consistently in the electrolyte model where the quantum solute and the surrounding solvent and electrolyte interact and mutually polarize. The electrostatics are determined by the solution of a generalized Poisson-Boltzmann equation via our highly parallel multigrid solver library DL_MG.

Our electrolyte model is able to treat molecules, entire biomolecules or larger nanoparticle assemblies in electrolyte as it has been implemented within open boundary conditions. We have also presented an implementation of the model for periodic boundary conditions, which is the first such electrolyte model under these boundary conditions in DFT to our knowledge: this allows one to treat extended systems such as electrode surfaces in contact with electrolyte. As this is a hybrid atomistic-continuum method it is necessary to avoid the possible (unphysical) accumulation of electrolyte charge near the quantum solute boundary. We have shown how we achieve this by employing accessibility functions that take into account the solute size as well as the solvation shell around the electrolyte ions. We have demonstrated how the model is calibrated against experimental mean activity coefficients to achieve good agreement with experimental measurements.

We expect that the electrolyte model we have developed here will open up the way for a multitude of applications in areas of high technological interest. These include applications in electrochemistry such as the development of new high capacity batteries (Li-ion batteries and beyond), heterogeneous catalysis, and the simulation of biomolecular systems (e.g. protein-ligand and protein-protein interactions relevant to drug design) as these are predominantly in electrolyte-containing solvent environments. Typically, complex systems with thousands of atoms are involved in these applications and these will be possible to tackle with the electrolyte model we presented here. Our model is implemented in the framework of linear-scaling DFT, which allows calculations with thousands of atoms, while conventional DFT is typically limited to a few hundred atoms.

As an example towards these future applications of our electrolyte model we have computed the electrolyte distribution in a model system representing the interface between a graphite anode with a Li atom intercalated at each of its two opposite edges in $LiPF_6$ electrolyte and ethylene carbonate solvent. This system consists of 1634 atoms and we studied two cases: where the Li atoms are intercalated at the graphite edge and where the Li atoms are well inside the solvent. We find that the presence of Li polarizes the surrounding electrolyte and we obtain both the electrolyte concentration locally around the surface and ions and its significant effect on the energetics of Li-intercalation into the graphite edge planes. We anticipate that more sophisticated model systems can be constructed and investigated in the future with such calculations to provide detailed information about the interfacial intercalation kinetics as a function of electrolyte concentration and potential (state of charge).

Appendix A: The excess chemical potential for the linearized P-BE with PBC

The linearization of the electrostatic contribution to the ionic chemical potential in the case of periodic boundary conditions is done as follows. Using Eq. 26 one can write

$$\frac{\mu_i^{\rm ex}}{k_{\rm B}T} = -\ln\left(\frac{I}{V\Gamma}\right) \ , \tag{64}$$

$$\text{where } I = \int_V \lambda(\mathbf{r}) \exp\left(-\frac{z_i\nu(\mathbf{r})}{k_{\rm B}T}\right) {\rm d}\mathbf{r} \ . \tag{65}$$

If $\left|\frac{z_i\nu(\mathbf{r})}{k_{\rm B}T}\right| \ll 1$ we can expand the exponential in the integral I and we have to first order:

$$\begin{aligned} I &\approx \int_V \lambda(\mathbf{r}) \left(1 - \frac{z_i\nu(\mathbf{r})}{k_{\rm B}T}\right) {\rm d}\mathbf{r} = \int_V \lambda(\mathbf{r})\, {\rm d}\mathbf{r} - \int_V \lambda(\mathbf{r}) \frac{z_i\nu(\mathbf{r})}{k_{\rm B}T} {\rm d}\mathbf{r} \\ &= \int_V \lambda(\mathbf{r}) {\rm d}\mathbf{r} \left(1 - \frac{\int_V \lambda(\mathbf{r}) \frac{z_i\nu(\mathbf{r})}{k_{\rm B}T} {\rm d}\mathbf{r}}{\int_V \lambda(\mathbf{r}) {\rm d}\mathbf{r}}\right) = \Gamma V \left(1 - \frac{1}{\Gamma V} \int_V \lambda(\mathbf{r}) \frac{z_i\nu(\mathbf{r})}{k_{\rm B}T} {\rm d}\mathbf{r}\right) , \end{aligned} \tag{66}$$

where we have used the definition of the electrolyte accessible volume $\Gamma V = \int_V \lambda(\mathbf{r}) {\rm d}\mathbf{r}$. Let us introduce the following average for the electrostatic potential:

$$\bar{\nu} = \frac{1}{V\Gamma} \int_V \lambda(\mathbf{r}) \nu(\mathbf{r}) {\rm d}\mathbf{r} \ . \tag{67}$$

With this notation the linear approximation for I, Eq. 65, can be written as follows:

$$I^{\rm lin} = V\Gamma \left(1 - \frac{z_i\bar{\nu}}{k_{\rm B}T}\right) . \tag{68}$$

Applying the expansion in first order systematically we can write the linear approximation for the electrostatic contribution to the ion chemical potential as follows:

$$\frac{\mu_i^{\rm ex}}{k_{\rm B}T} = -\ln\left(\frac{I}{V\Gamma}\right) \approx -\ln\left(\frac{I^{\rm lin}}{V\Gamma}\right) = -\ln\left(1 - \frac{z_i\bar{\nu}}{k_{\rm B}T}\right) \approx \frac{z_i\bar{\nu}}{k_{\rm B}T} \ . \tag{69}$$

In the above derivation we used $\ln(1+x) \approx x$ for $x \ll 1$ and the fact that

$$\left|\frac{z_i \nu(\mathbf{r})}{k_\mathrm{B}T}\right| \ll 1 \implies \left|\frac{z_i \bar{\nu}}{k_\mathrm{B}T}\right| \ll 1 \ . \tag{70}$$

Acknowledgement

This work was carried out with funding from the Faraday Institution (faraday.ac.uk; EP/S003053/1), grant number FIRG003. The majority of computations presented in this work were performed on the Iridis5 supercomputer of the University of Southampton and the Michael supercomputer of the Faraday Institution. We acknowledge the UK Materials and Molecular Modelling Hub for computational resources, partially funded by EPSRC (EP/P020194/1). JD acknowledges the support of the TASK Academic Computer Centre (Gdańsk, Poland), where some of the calculations were run. We would like to thank Dr Gilberto Teobaldi of STFC, Scientific Computing Department, Harwell for helpful discussions regarding the calculation of activity coefficients. We would like to thank Professor John Owen of the University of Southampton for helpful discussions.

References

(1) Łodziana, Z.; Topsøe, N. Y.; Nørskov, J. K. A negative surface energy for alumina. *Nature Materials* **2004**, *3*, 289–293.

(2) Hohenberg, P.; Kohn, W. Inhomogeneous Electron Gas. *Physical Review* **1964**, *136*, B864–B871.

(3) Kohn, W.; Sham, L. J. Self-Consistent Equations Including Exchange and Correlation Effects. *Physical Review* **1965**, *140*, A1133–A1138.

(4) Skylaris, C. K.; Haynes, P. D.; Mostofi, A. A.; Payne, M. C. Introducing ONETEP:

Linear-scaling density functional simulations on parallel computers. *Journal of Chemical Physics* **2005**, *122*, 1–10.

(5) Tomasi, J.; Mennucci, B.; Cammi, R. Quantum mechanical continuum solvation models. *Chemical Reviews* **2005**, *105*, 2999–3093.

(6) Miertuš, S.; Scrocco, E.; Tomasi, J. Electrostatic interaction of a solute with a continuum. A direct utilizaion of AB initio molecular potentials for the prevision of solvent effects. *Chemical Physics* **1981**, *55*, 117–129.

(7) Amovilli, C.; Barone, V.; Cammi, R.; Cancès, E.; Cossi, M.; Mennucci, B.; Pomelli, C. S.; Tomasi, J. In *Recent Advances in the Description of Solvent Effects with the Polarizable Continuum Model*; Löwdin, P.-O. B. T. A. i. Q. C., Ed.; Academic Press, 1998; Vol. 32; pp 227–261.

(8) Klamt, A.; Schüürmann, G. COSMO: a new approach to dielectric screening in solvents with explicit expressions for the screening energy and its gradient. *Journal of the Chemical Society, Perkin Transactions 2* **1993**, 799–805.

(9) Cancès, E.; Mennucci, B.; Tomasi, J. A new integral equation formalism for the polarizable continuum model: Theoretical background and applications to isotropic and anisotropic dielectrics. *The Journal of Chemical Physics* **1997**, *107*, 3032–3041.

(10) Zhan, C.-G.; Bentley, J.; Chipman, D. M. Volume polarization in reaction field theory. *The Journal of Chemical Physics* **1998**, *108*, 177–192.

(11) Kirkwood, J. G. The Dielectric Polarization of Polar Liquids. *The Journal of Chemical Physics* **1939**, *7*, 911–919.

(12) Onsager, L. Electric Moments of Molecules in Liquids. *Journal of the American Chemical Society* **1936**, *58*, 1486–1493.

(13) Still, W. C.; Tempczyk, A.; Hawley, R. C.; Hendrickson, T. Semianalytical treatment of solvation for molecular mechanics and dynamics. *Journal of the American Chemical Society* **1990**, *112*, 6127–6129.

(14) Cramer, C. J.; Truhlar, D. G. Implicit Solvation Models: Equilibria, Structure, Spectra, and Dynamics. *Chemical Reviews* **1999**, *99*, 2161–2200.

(15) Cortis, C. M.; Langlois, J.; Beachy, M. D.; Friesner, R. A. Quantum mechanical geometry optimization in solution using a finite element continuum electrostatics method. *The Journal of Chemical Physics* **1996**, *105*, 5472–5484.

(16) Warwicker, J. Continuum dielectric modelling of the protein-solvent system, and calculation of the long-range electrostatic field of the enzyme phosphoglycerate mutase. *Journal of Theoretical Biology* **1986**, *121*, 199–210.

(17) Womack, J. C.; Anton, L.; Dziedzic, J.; Hasnip, P. J.; Probert, M. I.; Skylaris, C. K. DL-MG: A Parallel Multigrid Poisson and Poisson-Boltzmann Solver for Electronic Structure Calculations in Vacuum and Solution. *Journal of Chemical Theory and Computation* **2018**, *14*, 1412–1432.

(18) Foresman, J. B.; Keith, T. A.; Wiberg, K. B.; Snoonian, J.; Frisch, M. J. Solvent Effects. 5. Influence of Cavity Shape, Truncation of Electrostatics, and Electron Correlation on ab Initio Reaction Field Calculations. *The Journal of Physical Chemistry* **1996**, *100*, 16098–16104.

(19) Fattebert, J. L.; Gygi, F. Density functional theory for efficient ab initio molecular dynamics simulations in solution. *Journal of Computational Chemistry* **2002**, *23*, 662–666.

(20) Scherlis, D. A.; Fattebert, J. L.; Gygi, F.; Cococcioni, M.; Marzari, N. A unified electrostatic and cavitation model for first-principles molecular dynamics in solution. *Journal of Chemical Physics* **2006**, *124*.

(21) Dziedzic, J.; Helal, H. H.; Skylaris, C. K.; Mostofi, A. A.; Payne, M. C. Minimal parameter implicit solvent model for ab initio electronic-structure calculations. *Epl* **2011**, *95*, 1–6.

(22) Dziedzic, J.; Fox, S. J.; Fox, T.; Tautermann, C. S.; Skylaris, C. K. Large-scale DFT calculations in implicit solvent - A case study on the T4 lysozyme L99A/M102Q protein. *International Journal of Quantum Chemistry* **2013**, *113*, 771–785.

(23) Andreussi, O.; Dabo, I.; Marzari, N. Revised self-consistent continuum solvation in electronic-structure calculations. *Journal of Chemical Physics* **2012**, *136*.

(24) Grochowski, P.; Trylska, J. Continuum molecular electrostatics, salt effects, and counterion binding – A review of the Poisson-Boltzmann theory and its modifications. *Biopolymers* **2008**, *89*, 93–113.

(25) Ren, P.; Chun, J.; Thomas, D. G.; Schnieders, M. J.; Marucho, M.; Zhang, J.; Baker, N. A. Biomolecular electrostatics and solvation: A computational perspective. *Quarterly Reviews of Biophysics* **2012**, *45*, 427–491.

(26) Borukhov, I.; Andelman, D.; Orland, H. Steric Effects in Electrolytes: A Modified Poisson-Boltzmann Equation. *Phys. Rev. Lett.* **1997**, *79*, 435–438.

(27) Borukhov, I.; Andelman, D.; Orland, H. Adsorption of large ions from an electrolyte solution: A modified Poisson-Boltzmann equation. *Electrochimica Acta* **2000**, *46*, 221–229.

(28) Jinnouchi, R.; Anderson, A. B. Electronic structure calculations of liquid-solid interfaces: Combination of density functional theory and modified Poisson-Boltzmann theory. *Phys. Rev. B* **2008**, *77*, 245417.

(29) Ringe, S.; Oberhofer, H.; Hille, C.; Matera, S.; Reuter, K. Function-Space-Based Solu-

tion Scheme for the Size-Modified Poisson-Boltzmann Equation in Full-Potential DFT. *Journal of Chemical Theory and Computation* **2016**, *12*, 4052–4066.

(30) Ringe, S.; Oberhofer, H.; Reuter, K. Transferable ionic parameters for first-principles Poisson-Boltzmann solvation calculations: Neutral solutes in aqueous monovalent salt solutions. *Journal of Chemical Physics* **2017**, *146*.

(31) Nattino, F.; Truscott, M.; Marzari, N.; Andreussi, O. Continuum models of the electrochemical diffuse layer in electronic-structure calculations. *The Journal of Chemical Physics* **2019**, *150*, 41722.

(32) Born, M.; Oppenheimer, R. Zur Quantentheorie der Molekeln. *Annalen der Physik* **1927**, *389*, 457–484.

(33) Sharp, K. A.; Honig, B. Calculating total electrostatic energies with the nonlinear Poisson-Boltzmann equation. *The Journal of Physical Chemistry* **1990**, *94*, 7684–7692.

(34) Fogolari, F.; Brigo, A.; Molinari, H. The Poisson–Boltzmann equation for biomolecular electrostatics: a tool for structural biology. *Journal of Molecular Recognition* **2002**, *15*, 377–392.

(35) Mathew, K.; Hennig, R. G. Implicit self-consistent description of electrolyte in plane-wave density-functional theory. *arXiv e-prints* **2016**, arXiv:1601.03346.

(36) Gray, C. G.; Stiles, P. J. Nonlinear electrostatics: the Poisson–Boltzmann equation. *European Journal of Physics* **2018**, *39*, 053002.

(37) Ruiz-Serrano, Á.; Skylaris, C. K. A variational method for density functional theory calculations on metallic systems with thousands of atoms. *Journal of Chemical Physics* **2013**, *139*.

(38) Fisicaro, G.; Genovese, L.; Andreussi, O.; Mandal, S.; Nair, N. N.; Marzari, N.;

Goedecker, S. Soft-Sphere Continuum Solvation in Electronic-Structure Calculations. *Journal of Chemical Theory and Computation* **2017**, *13*, 3829–3845.

(39) Sundararaman, R.; Letchworth-Weaver, K.; Schwarz, K. A. Improving accuracy of electrochemical capacitance and solvation energetics in first-principles calculations. *Journal of Chemical Physics* **2018**, *148*.

(40) Stein, C. J.; Herbert, J. M.; Head-Gordon, M. The Poisson-Boltzmann model for implicit solvation of electrolyte solutions: Quantum chemical implementation and assessment via Sechenov coefficients. *Journal of Chemical Physics* **2019**, *224111*.

(41) Ruiz Serrano, A.; Hine, N. D. M.; Skylaris, C.-K. Pulay forces from localized orbitals optimized in situ using a psinc basis set. *The Journal of Chemical Physics* **2012**, *136*, 234101.

(42) Skylaris, C.-K.; Mostofi, A. A.; Haynes, P. D.; Diéguez, O.; Payne, M. C. Nonorthogonal generalized Wannier function pseudopotential plane-wave method. *Phys. Rev. B* **2002**, *66*, 035119.

(43) Hine, N. D. M.; Dziedzic, J.; Haynes, P. D.; Skylaris, C.-K. Electrostatic interactions in finite systems treated with periodic boundary conditions: Application to linear-scaling density functional theory. *J. Chem. Phys.* **2011**, *135*, 204103.

(44) Atkins, P. W.; De Paula, J. *Atkins' Physical chemistry, 9th Ed.*; 2014.

(45) *http://www.dlmg.org*

(46) Mostofi, A. A.; Haynes, P. D.; Skylaris, C.-K.; Payne, M. C. Preconditioned iterative minimization for linear-scaling electronic structure calculations. *The Journal of Chemical Physics* **2003**, *119*, 8842–8848.

(47) Mostofi, A. A. *On Linear-scaling Methods for Quantum Mechanical First-principles Calculations*; University of Cambridge, 2004.

(48) Womack, J. C.; Anton, L.; Dziedzic, J.; Hasnip, P. J.; Probert, M. I. J.; Skylaris, C.-K. *Implementation and optimisation of advanced solvent modelling functionality in CASTEP and ONETEP*; 2017; http://www.archer.ac.uk/community/eCSE/eCSE07-06/eCSE07-06.php.

(49) Hamer, W. J.; Yung-Chi, Y. Osmotic Coefficients and Mean Activity Coefficients of Uni-univalent Electrolytes in Water at 25°C. *Journal of Physical and Chemical Reference Data* **1972**, *1*, 1047–1100.

(50) Stewart, S.; Newman, J. Measuring the salt activity coefficient in lithium-battery electrolytes. *Journal of the Electrochemical Society* **2008**, *155*, 458–463.

(51) Debye, P.; Hückel, E. On the theory of electrolytes. II Limiting law for electric conductivity. *Physikalische Zeitschrift* **1923**, *24*, 305–325.

(52) Hall, D. S.; Self, J.; Dahn, J. R. Dielectric Constants for Quantum Chemistry and Li-Ion Batteries: Solvent Blends of Ethylene Carbonate and Ethyl Methyl Carbonate. *Journal of Physical Chemistry C* **2015**, *119*, 22322–22330.

(53) Naejus, R.; Damas, C.; Lemordant, D.; Coudert, R.; Willmann, P. Excess thermodynamic properties of the ethylene carbonate-trifluoroethyl methyl carbonate and propylene carbonate-trifluoroethyl methyl carbonate systems at T = (298.15 or 315.15) K. *Journal of Chemical Thermodynamics* **2002**, *34*, 795–806.

(54) Seo, D. M.; Reininger, S.; Kutcher, M.; Redmond, K.; Euler, W. B.; Lucht, B. L. Role of Mixed Solvation and Ion Pairing in the Solution Structure of Lithium Ion Battery Electrolytes. *The Journal of Physical Chemistry C* **2015**, *119*, 14038–14046.

(55) Bhandari, A.; Gupta, P. K.; Bhattacharya, J.; Pala, R. G. S. Higher Energy Barrier for Interfacial Li-Ion Transfer from EC/LiPF6 Electrolyte into (010) LiFePO4 Cathode Surface than Bulk Li-Ion Diffusion within Both Cathode and Electrolyte. *Journal of The Electrochemical Society* **2019**, *166*, A2966–A2972.

(56) Humphrey, W.; Dalke, A.; Schulten, K. VMD: Visual molecular dynamics. *Journal of Molecular Graphics* **1996**, *14*, 33 – 38.

TOC Graphic